TEMPERED FRACTIONAL DERIVATIVE:

APPLICATION TO LINEAR FLOW

A Thesis

by

XI YANG

Submitted to the Office of Graduate and Professional Studies of
Texas A&M University
in partial fulfillment of the requirements for the degree of

MASTER OF SCIENCE

Chair of Committee,	Peter Valkó
Committee Members,	Thomas A. Blasingame
	Kan Wu
Head of Department,	Jeff Spath

August 2018

Major Subject: Petroleum Engineering

ABSTRACT

Hydraulic fracturing has become the dominant completion method in unconventional shale oil and gas reservoirs. The fluid flow inside unconventional shale reservoirs is different compared to conventional reservoirs. The importance of understanding anomalous diffusion of unconventional reservoir starts to appear. Traditional Darcy's law is not appropriate to describe sub-diffusion behavior. In order to analytically model the sub-diffusion behavior, continuous time random walk (CTRW) theory is introduced in some literature. Fractional derivative method is used to apply CTRW theory to the flux law and thus modelling sub-diffusion behavior. For flow into fracture in unconventional reservoir, linear flow regime is suitable not only for transient period but also for late-time period. Applying fractional derivative to the flux law successfully describes the sub-diffusion behavior in transient period. However, the flux law using fractional derivative causes inaccurate result for late-time period. In order to ameliorate the problem, we introduce a tempering factor into the fractional derivative. Then, tempering fractional derivative is applied to the flux law. This flux law is applied to linear flow diffusivity equation and transferred into Laplace domain for solution. Real time domain solutions are obtained using GWR numerical inversion. In our study, model for single fracture is successfully created for two different boundary conditions. After verifying our model with numerical model and fractional linear flow model, we are generating type curves for various fractional parameter and tempering factor parameter pairs. Furthermore, we analyze production data from three oil wells in Eagle Ford shale play using our tempered fractional linear flow model.

DEDICATION

I dedicate this work to all my family members.

ACKNOWLEDGEMENTS

I would like to express my gratitude to my committee chair, Dr. Peter Valkó, for his patient guidance and support throughout this research. I would also like to thank my committee member, Dr. Thomas A. Blasingame, and my committee member, Dr. Kan Wu for their help on data searching and abundant information.

Thanks also go to all faculties and staffs of Texas A&M University Petroleum Engineering Department.

I would like to thank my parents, Kai Yang and Li Liu, who gave strongly supported me during these two years and always guided me to explore more.

Finally, I would like to thank all my friends who have helped me during these two years. I would especially like to thank Gongzhan Hua, Ding Ma, and Yuqi Hu. They listened to me and encouraged me in hard times, and cheered with me for joyful moments.

CONTRIBUTORS AND FUNDING SOURCES

This work was supervised by a thesis committee consisting of Dr. Peter Valkó, Dr. Thomas A. Blasingame, and Dr. Kan Wu.

Graduate study was supported by an in-state tuition fellowship from Department of Petroleum Engineering at Texas A&M University.

The data analyzed for the Results and Discussion section was extracted from SPE papers found on OnePetro. The software Mathematica is used for equation solving, numerical Laplace inversion, and plotting. The software CMG is used for generating numerical model results.

All other work conducted for the thesis was completed by the student independently.

TABLE OF CONTENTS

Page

LIST OF FIGURES

LIST OF TABLES

1. INTRODUCTION

Nowadays, horizontal wells with multiple fractures are common for oil and gas recovery from unconventional tight shale reservoirs. Though numerical models plays an important role in unconventional reservoir simulation and yields accurate results, the high computational cost let some operators unable to apply numerical models to forecast production. On the other hand, analytical models are suitable for performing prediction with acceptable computational cost. Many successful models are constructed based on a combination of the conservation equation, the Darcy flux law, and an equation of state for the fluid in the pores (Raghavan, 2011). As we know, Darcy flux law is based on classical diffusion pattern. For unconventional reservoir, the rock fabric is complex with disordered structures, rough interfaces, and so on (Raghavan, 2011). Thus, the fluid flow through this complex rock fabric may not follow classical diffusion. Instead, anomalous diffusion is used to describe the abnormal fluid flow behavior.

1.1 Classical Diffusion & Random Walk

The movement of fluid particles of classical diffusion can be described as random walks in the sense that the displacement of a particle may be described by a sum of independent displacements over short intervals of time following a distribution with well-defined variance (Raghavan, 2012). In another word, a particle or a walker waits for a fixed time step before each travel, and the travel distance follows a certain distribution (Vlahos et al.,

2008). For the simplest classical diffusion model, the travel distance is a fixed value one, and the walker only move up or down randomly with equivalent probability. The result for this simple 1-D case is shown in Fig. 1.1. Since each step of walk is equally likely to move up or down, we can see that the displacements are random variables with zero mean. From this simplest example, the key equation of random walk can be shown in Eq. 1.1 below.

$$\langle(\Delta x)^2\rangle \propto t \quad \text{.....(1.1)}$$

In Eq. 1.1, Δx is the displacement of the walker, and the angle brackets represents the mean value calculation. Thus, $\langle(\Delta x)^2\rangle$ is the mean square displacement, and it is proportional to time. In more sophisticated models, the travel length of every step may follow a certain distribution. While the direction of travel in one dimensional random walk is either up or down with equal probability of 1/2, the mean value for the displacements will be zero all the time. Moreover, the waiting time between two subsequent steps of walk is constant, which means the time is only a dummy variable or a counter in random walk models (Vlahos et al., 2008). Random walk has been successfully used to model classical diffusion including Fick's law and Darcy's law. However, for random walk, the step size is relatively small, and the particles will not take large steps during the process. While classical diffusion describes many aspects of flow in porous media, it has serious limitations, especially when the micro structure of the solid medium is highly heterogeneous and the characteristic scale of the pore structure is so small that the nature of the flowing fluid particle size is not negligible.

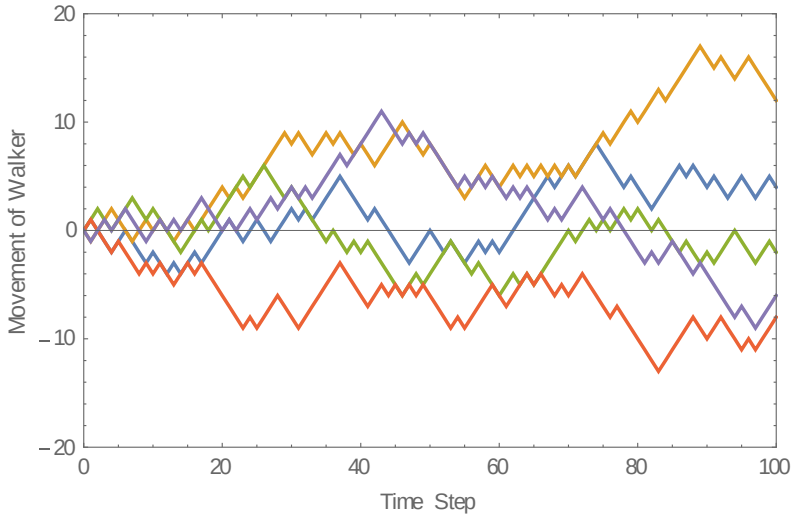

Figure 1.1 - Simple random walk example in one dimension as a function of time.

1.2 Anomalous Diffusion & Continuous Time Random Walk (CTRW)

When the main characteristic of the normal diffusion process (Equ 1.1) is not valid, we speak about anomalous diffusion. A modification of the simplest random walk model, called Continuous Time Random Walk (CTRW) is capable to describe processes of anomalous diffusion. In a CTRW, the waiting time is not constant, but a random variable with a given distribution. Moreover, the length of the step can also be a random variable, and depending on the actual distribution used, the step size could be very large. The "large" step in a finite system means large up to system size, and for infinite system, "large" means that the step length of walkers are unlimited (Vlahos et al., 2008). In order to achieve this goal, the waiting time between two steps of a walker should not be fixed. Since now the step length and the waiting time between steps are both random and follow

certain distributions, the classical random walk model becomes continuous random walk (CTRW). In another word, CTRW is a generalization of a random walk where the walker waits for a random time between jumps (Klages et al., 2008; Paul and Baschnagel, 2013). Thus, Eq. 1.1 now can be modified to the following form as shown in Eq. 1.2.

$$\langle (\Delta x)^2 \rangle \propto t^{\alpha} \quad \text{.....(1.2)}$$

As shown in Eq. 1.2, mean square displacement is proportional to the time to the power of α. When alpha is not equal to one, Eq. 1.2 represents the basis of anomalous diffusion. Specifically, if $\alpha > 1$, the diffusion process becomes super-diffusion, and if $\alpha < 1$, the diffusion process becomes sub-diffusion (Balescu, 1998). Also, when $\alpha = 1$, Eq. 1.2 will be same as Eq. 1.1 which represents normal diffusion. As shown in Fig. 1.2a by Vlahos et al. (2008), we can observe that for normal diffusion, the particle keeps moving with relatively small step length. In Fig. 1.2b, the particle will have long "flights" after being trapped for a certain time. While using CTRW to model anomalous diffusion behavior for unconventional petroleum reservoir like tight shale reservoir, we focus on sub-diffusion with $\alpha < 1$.

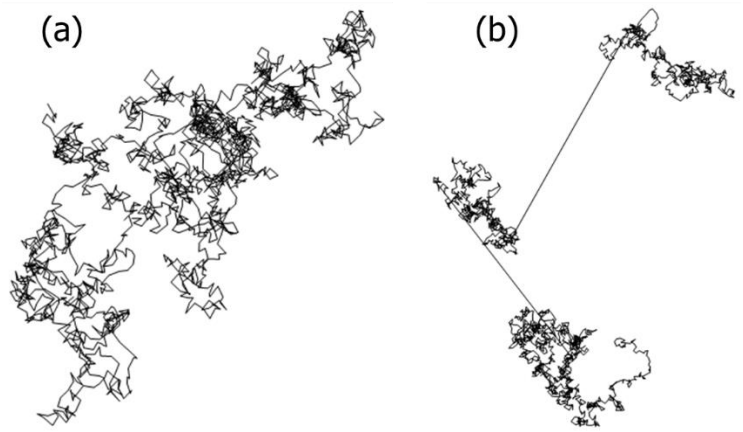

Figure 1.2 - Comparison between normal diffusion and anomalous diffusion (Vlahos et al., 2018): (a) Normal Diffusion: Random walk in dynamical systems close to equilibrium; (b) Anomalous diffusion: Random walk in dynamical systems far from equilibrium.

1.3 Application of tempering factor

Applying CTRW theory to the flux law of petroleum engineering needs fractional calculus and has been investigated in great details in recent years (Raghavan, 2011; Rhagavan, 2012; Rhagavan and Chen, 2013; Chen and Raghavan, 2015; Albinali et al., 2016; Holy, 2016; Holy and Ozkan, 2016a; Holy and Ozkan, 2016b; Raghavan and Chen, 2017). Raghavan and Chen (2017) introduced an analytical time-fractional 1-D linear flow single phase model. Holy and Ozkan (2016) developed a numerical model of multiphase linear flow, which used time-fractional derivative for sub-diffusion behavior and space-fractional derivative for super-diffusion. Though these models are suitable for capturing the peculiar behavior of transient flow in unconventional reservoirs, they show contradictory, or at least less than intuitive results for late times. Also, even for transient

periods, the only parameter alpha is not sufficient to model and explain the complex fluid flow characteristics emerging in unconventional reservoirs. Thus, we choose to introduce a tempering factor to overcome the shortcomings of fractional derivate.

The tempering factor has been already applied in the field of groundwater flow by Meerschaert et al. (2008) who used tempered anomalous diffusion (TAD) in heterogeneous systems. Meerschaert et al. (2002) found that time-fractional advection dispersion models employ stable waiting time, and sub-diffusive effect can be modeled with long power-law waiting time distribution. However, after using space-fractional model for super-diffusion and using time-fractional model for sub-diffusion, problems are found with matching the power-law tails of these models with experimental or numerical simulations data (Meerschaert et al., 2002; Schumer et al., 2003; Cartea and del-Castillo-Nergrete, 2007; Zhang et al., 2007). In order to solve this problem, Meerschaert et al. (2008) temper the distribution of waiting times between particle jumps. As a result of tempering, the TAD model contains both the time-fractional diffusion behavior at early times and the classical diffusion behavior at late times (Schumer 2003). In another word, the tempering factor effectively controls the time when the model behavior changes from fractional to classical (Meerschaert et al., 2008). TAD model is proved to be useful and accurate by both numerical simulations and observed data. Zhang and Lv (2007) demonstrate TAD model can capture the movement of passive tracers in natural heterogeneous media successfully. Kelly et al. (2017) compared TAD model with space-fractional advection-dispersion equation (sFADE) and fractional mobile-immobile (FMIM) equation using observed data from in-stream pulse injection experiments

conducted in the Selke Rived (Schmadel et al., 2016). The results showed that though sFADE and FMIM matched observed data better than classical model based on Fick's Law, TAD model captured even the late-time truncation of the power law and gave the most accurate result (Kelly et al., 2017).

The water resources literature documented many sub-diffusive behavior (Haggerty et al., 200). Thus, Meerschaert et al. (2008) believe that the TAD model can be applied broadly.

Recently, the petroleum engineering literature has been focusing on unconventional reservoirs stimulated by hydraulic fracturing techniques. Several authors have suggested that production from such reservoirs show sub-diffusion behavior as well (Raghavan and Chen, 2017). Since in the water resources applications the tempered fractional version of Fick's Law outperforms the time fractional model in many respects, it appears natural to apply the tempered fractional derivative to Darcy flux law in order to develop a model, which has sub-diffusion behavior in early-time and smooth transition to normal diffusion in late time.

2. METHODOLOGY

In this work we propose a process including the following steps:

1. Use tempered fractional derivative to change Darcy flux for sub-diffusion behavior.

2. Combine the new flux law with linear flow diffusivity equation.

3. Transform the equation into Laplace domain and derive the solution analytically.

4. Perform numerical inverse Laplace transform to obtain the results in time domain.

2.1 Foundation of flux law

According to the four general steps showing above, the first step should be apply tempered fractional derivative to traditional Darcy's flux law. In that case, we can use the new flux law to model sub-diffusion behavior. Recall Eq. 1.1 in the introduction part

$$\langle (\Delta x)^2 \rangle \propto t \quad \text{.....(1.1)}$$

With the mean square displacement proportional to time, traditional Darcy's law is valid that is

$$v(x,t) = -\frac{k}{\mu}\nabla p(x,t) \quad \text{.....(2.1)}$$

For CTRW, since the walker waits for a random time between jumps, Eq. 1.1 is modified to Eq. 1.2 in the introduction part. Recall Eq. 1.2 that is

$$\langle (\Delta x)^2 \rangle \propto t^{\alpha} \quad \text{.....(1.2)}$$

When the power α in Eq. 1.2 is smaller than one, the diffusion process is sub-diffusion, which is the behavior we anticipate to appear in tight shale reservoir. Thus, Darcy's flux law shown in Eq. 2.1 needs to be modified to

$$v(x,t) = -\left(\frac{k}{\mu}\right)\frac{\partial^{1-\alpha}}{\partial t^{1-\alpha}}[\nabla p(x,t)] \quad \text{(2.2)}$$

where the $\left(\frac{k}{\mu}\right)$ factor has $\frac{m^2}{Pa\cdot s}$ unit in the case of α= 0, and $\frac{m^2}{Pa\cdot s^{1-\alpha}}$ for non-zero alpha (Raghavan and Chen, 2017). The flux law shown in Eq. 2.2 is one of the foundation of this research work.

2.2 Fractional Derivative and Laplace Transformation

In last part, the derivative part of the right-hand-side of Eq. 2.2 is fractional derivative. The definition of fractional derivative was introduced by Mathematicians dated back to last century (Ross, 1975; Debnath, 2004). However, the research on fractional calculus remains on theory until recent fifteen years. The definition of fractional derivative is shown in Eq. 2.3 below.

$$\frac{d^\alpha}{dt^\alpha}f(t) = \frac{1}{\Gamma(1-\alpha)}\int_0^t dt'(t-t')^{-\alpha}\frac{d}{dt'}f(t') \quad \text{(2.3)}$$

Or in some other literature, the fractional derivative is shown as Eq. 2.4 (Meerschaert et al., 2015; Sabzikar et al., 2014).

$$D_t^\alpha f(t) = \frac{1}{\Gamma(1-\alpha)}\int_0^\infty [f(t) - f(t-t')]\, t'^{-\alpha-1}\, dt' \quad \text{(2.4)}$$

In Eq. 2.3 and 2.4, Γ means the gamma function and t' is a dummy variable. Mathematically, these two equations are the same. In real time domain, the right hand side of Eq. 2.3 and 2.4 seems impossible to calculate during application to complex functions. Thus, Fourier transformation or Laplace transformation is always associated with the application of fractional derivative. For our research we focus on the Laplace transform of the fractional derivative. According to Mathai (2006) the Laplace transform of the time fractional derivative is

$$L\left\{\frac{d^{\alpha}}{dt^{\alpha}}f(t)\right\} = s^{\alpha}F(s) - \sum_{k=1}^{n} s^{k-1}\frac{d^{\alpha-k}}{dt^{\alpha-k}}f(0+) \quad \text{.....(2.5)}$$

For our usage of Laplace transform of fractional derivative, the initial condition will be zero. So Eq. 2.5 can be further simplified to the form below.

$$L\left\{\frac{d^{\alpha}}{dt^{\alpha}}f(t)\right\} = s^{\alpha}F(s) \quad \text{.....(2.6)}$$

2.3 Tempered Fractional Derivative and Laplace Transformation

The application of fractional derivative to linear flow has been already carried out, see e.g. Raghavan (2011), Rhagavan (2012), Rhagavan and Chen (2013), Chen and Raghavan (2015), and Raghavan and Chen (2017). In this research work, we add a tempering factor to the fractional derivative. The tempered fractional derivative is based on the fractional derivative. Tempered fractional derivative can be understood by its most important application to model diffusion, which is called tempered fractional diffusion by Sabzikar

et al. (2014). It adds an exponential tempering factor to the particle jump density of the random walk model, effectively stating that very long waiting times between the jumps are extremely unlikely. This tempering factor is defined as

$\lambda_\varepsilon = D\left(\frac{\alpha}{\Gamma(1-\alpha)}\right) C_\varepsilon$ where $C_\varepsilon = \int_\varepsilon^\infty t'^{-\alpha-1} e^{-\lambda t'} dt'$ for any $\varepsilon > 0$..... (2.7)

where λ is a new parameter of dimension 1/time.

For our purpose, while using tempered fractional derivative, the fractional factor α is between 0 and 1 and the λ parameter is positive. The form of tempered fractional derivative is

$D_t^{\alpha,\lambda} f(t) = \frac{1}{\Gamma(1-\alpha)} \int_0^\infty [f(t) - f(t-t')]\, e^{-\lambda t'}\, t'^{-\alpha-1}\, dt'$..... (2.8)

We know that Laplace transform of $e^{\lambda t} f(t)$ is $F(s-\lambda)$. Applying the shift property of Laplace transform on fractional derivative we can get

$\int_0^\infty e^{-st} D_t^\alpha \left[e^{\lambda t} f(t)\right] dt = s^\alpha F(s-\lambda)$..... (2.9)

Using the shift property in Eq. 2.9 once more we get

$\int_0^\infty e^{-st} e^{-\lambda t}\, D_t^\alpha \left[e^{\lambda t} f(t)\right] dt = (s+\lambda)^\alpha F(s)$ ..... (2.10)

Thus, with the assumption of $0 < \alpha < 1$, the *tempered fractional derivative* can be defined as

$D_t^{\alpha,\lambda}[f(t)] = e^{-\lambda t}\, D_t^{\alpha,}\left[e^{\lambda t} f(t)\right] - \lambda^\alpha f(t)$..... (2.11)

Also, we can obtain the Laplace transform of the tempered fractional derivative as

$$L\left\{ D_t^{\alpha,\lambda}[f(t)]\right\} = [(s+\lambda)^{\alpha} - \lambda^{\alpha}]\, F(s) \quad \text{.....(2.12)}$$

For Eq. 2.12, we need to assume zero initial condition as well. Otherwise, there will be another term depending on the initial condition.

2.4 Diffusivity Equation

Linear flow has many forms and extensions like bi-linear flow. We choose to use linear formation flow regime for our model. Linear formation flow only considers the flow from the formation into fracture, which means we assume the fracture conductivity is infinite. Wattenbarger et al. (1998) defines that when dimensionless conductivity, defined in Eq. 2.13, is bigger than 50, the assumption of infinite fracture conductivity is a good assumption.

$$F_{CD} = \frac{k_f w_f}{k L_f} \quad \text{.....(2.13)}$$

In reality, in tight shale reservoirs like Eagle Ford, the equivalent permeability of the formation within the stimulated volume of the reservoir will be lower than 0.0002 md (Wang and Liu, 2011; Agboada and Ahmadi, 2013; Gong et al., 2013). Moreover, the hydraulic fracture permeability with 0.2-inch fracture width is between 50 to 120 md, and the typical half fracture length is longer than 80 ft (Gong et al., 2013). Thus, the dimensionless fracture conductivity shown in Eq. 2.13 will be higher than 50 for the

typical tight shale reservoir, which means our assumption of infinite hydraulic fracture conductivity will not affect the accuracy of our model.

The diffusivity equation of a slightly compressible fluid in a linear formation flow system corresponding to the flux law in Eq. 2.2 now becomes

$$\frac{\partial}{\partial x}\left[\left(\frac{k}{\mu}\right)\frac{\partial}{\partial x}(p(x,t)\right] = \phi c\,\frac{\partial^{\alpha}}{\partial t^{\alpha}}(p(x,t) \quad \text{.....(2.14)}$$

Assuming permeability k and viscosity μ does not change with position, we can get

$$\frac{\partial}{\partial x}\left[\frac{\partial}{\partial x}p(x,t)\right] = \phi c\left(\frac{\mu}{k}\right)\frac{\partial^{\alpha}}{\partial t^{\alpha}}p(x,t) \quad \text{.....(2.15)}$$

Eq. 2.15 is the sub-diffusive fractional model of linear flow.

When exponential tempering with parameter λ is considered, the time derivative on the right hand side is replaced by the tempered time derivative:

$$\frac{\partial}{\partial x}\left[\frac{\partial}{\partial x}p(x,t)\right] = \phi c\left(\frac{\mu}{k}\right)\,D_t^{\alpha,\lambda}[p(x,t)] \quad \text{.....(2.16)}$$

We will transform Eq. 2.16 into Laplace domain after introducing dimensionless variables.

2.5 Define Dimensionless Variables

Before transforming Eq. 2.16 into Laplace space, it is convenient to introduce dimensionless variables. The purpose of using dimensionless variables is that

dimensionless variables are useful to generate type curves. Moreover, when we analyze field data and compare to type curves, we can easily compute dimensionless variables using reservoir and fracture parameters.

In this research, our model is developed for a rectangle region, which is a quarter production region of a fracture as shown in Fig. 2.1. For linear flow regime, this model can be easily extended to the whole fracture because the production rate of the whole fracture will be four times of this quarter region.

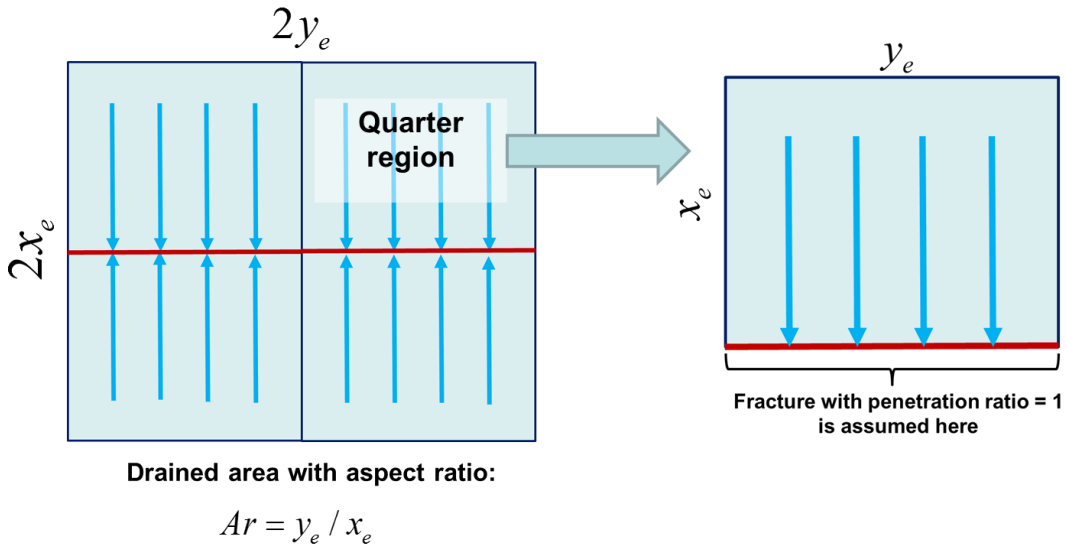

Figure 2.1 - Quarter region linear flow model of a single fracture.

The first dimensionless variable we need to define is dimensionless distance. In Eq. 2.16, x is the distance from the fracture. In order to make this distance, x to be dimensionless, we need to divide it by a characteristic distance, L as shown in Eq. 2.17 below.

$$x_D = \frac{x}{L} \text{ or } x = L\, x_D \quad \text{.....(2.17)}$$

Applying the definition of dimensionless distance to Eq. 2.16, we can get

$$\frac{\partial}{\partial L\, x_D}\left[\frac{\partial}{\partial L\, x_D} p(x,t)\right] = \frac{\phi \mu c}{k}\frac{\partial^\alpha}{\partial t^\alpha} p(x,t). \quad \text{.....(2.18)}$$

Eq. 2.18 can be furtherly simplified to Eq. 2.19 below by factoring out the characteristic distance, L and then rearrange the equation.

$$\frac{\partial}{\partial x_D}\left[\frac{\partial}{\partial x_D} p(x,t)\right] = \frac{\phi \mu c L^2}{k}\frac{\partial^\alpha}{\partial t^\alpha} p(x,t) \quad \text{.....(2.19)}$$

Now, we need to define the characteristic distance, L. For vertical well with radial flow, the characteristic distance is defined as wellbore radius. For linear flow, Wattenbarger et al. (1998) defines the characteristic distance to be fracture half length x_f . In this study, we choose to use a different definition of characteristic distance based on the drainage area. In this case, we can couple our model with different aspect ratio of drainage area.

$$L = \sqrt{x_e\, y_e} \quad \text{.....(2.20)}$$

In Eq. 2.20, y_e and x_e are the corresponding length and width of the rectangle drainage area. The drainage area length, y_e is parallel to the hydraulic fracture, and the drainage area width x_e is perpendicular to the hydraulic fracture. Since we only consider linear formation flow in this study, penetration ratio of fracture in the drainage area is not important so the penetration ratio remains one in our model. Eq. 2.20 shows that our

characteristic distance is the square root of drainage area. Thus, we can then define the dimensionless aspect ratio as

$$Ar = \frac{y_e}{x_e}. \quad (2.21)$$

Clearly, we can conclude the relationship between drainage area length, y_e and characteristic, L as well as the relationship between drainage area width, x_e and characteristic, L shown in Eq. 2.22 and 2.23 below.

$$y_e = L\sqrt{Ar} \quad (2.22)$$

$$x_e = L/\sqrt{Ar} \quad (2.23)$$

Combining Eq. 2.22 and 2.23 with the definition of dimensionless distance shown in Eq. 2.17, we can obtain the dimensionless length, y_{eD} and width, x_{eD} shown in Eq. 2.24 and 2.25 below.

$$y_{eD} = \sqrt{Ar} \quad (2.24)$$

$$x_{eD} = 1/\sqrt{Ar} \quad (2.25)$$

Besides dimensionless distance, we need to define dimensionless pressure. Similar as dimensionless distance, we need the pressure to be divided by a characteristic pressure (Raghavan, 1998). The definition of dimensionless pressure is given in Eq. 2.26 below.

$$p_D = \frac{1}{p_{ch}}(p_i - p) \text{ or } p = p_i - p_{ch}p_D \quad (2.26)$$

In Eq. 2.26, p_i is initial reservoir pressure, and p_{ch} is characteristic pressure. For different boundary conditions, the characteristic pressure will be different, which will be discussed later. Now, we apply dimensionless pressure shown in Eq. 2.26 to Eq. 2.19, we can obtain

$$\frac{\partial}{\partial x_D}\left[\frac{\partial}{\partial x_D}(p_i - p_{ch}p_D)\right] = \frac{\phi\mu c L^2}{k}\frac{\partial^\alpha}{\partial t^\alpha}(p_i - p_{ch}p_D) \quad \text{.....(2.27)}$$

Reducing the characteristic pressure, p_{ch} on both sides of Eq. 2.27 and rearranging the equation, we can get the time-fractional diffusivity equation as

$$\frac{\partial}{\partial x_D}\left[\frac{\partial p_D}{\partial x_D}\right] = \frac{\phi\mu c L^2}{k}\frac{\partial^\alpha p_D}{\partial t^\alpha} \quad \text{.....(2.28)}$$

The last dimensionless variable to be determined is the dimensionless time. In Eq. 2.28, we can put the remaining parameters on the right-hand-side of the equation to dimensionless time. Thus, dimensionless time is defined as

$$t^\alpha = \frac{\phi\mu c L^2}{k}{t_D}^\alpha \text{ or } {t_D}^\alpha = \frac{k}{\phi\mu c L^2}t^\alpha. \quad \text{.....(2.29)}$$

Applying the definition of dimensionless time shown in Eq. 2.29 to diffusivity equation shown in Eq. 2.28, we can obtain the final form of dimensionless diffusivity equation as

$$\frac{\partial}{\partial x_D}\left[\frac{\partial p_D}{\partial x_D}\right] = \frac{\partial^\alpha p_D}{\partial {t_D}^\alpha} \quad \text{.....(2.30)}$$

Eq. 2.30 is the foundation of our model. We will solve this dimensionless diffusivity equation with different boundary conditions. As mentioned in the proposed four steps of methodology, the third step is transforming diffusivity equation shown in Eq. 2.30.

If we apply fractional derivative theory (without tempering factor) introduced in section 2.3 and perform Laplace transform w.r.t time on Eq. 2.30, with zero initial condition, we can get

$$\frac{\partial}{\partial x_D}\left[\frac{\partial}{\partial x_D}\left(\bar{p}_D\right)\right] = s^{\alpha}\,\bar{p}_D \quad (2.31)$$

If we apply tempered fractional derivative theory introduced in section 2.3 and perform Laplace transform w.r.t time on Eq. 2.30, with zero initial condition, we can get

$$\frac{\partial}{\partial x_D}\left[\frac{\partial}{\partial x_D}\left(\frac{s}{(s+\lambda)^{\alpha}-\lambda^{\alpha}}\bar{p}_D\right)\right] = s\,\bar{p}_D \quad (2.32)$$

where s is transformed complex variable in Laplace domain; λ is the tempering factor; α is fractional derivative parameter; $\bar{p}_D$ is the transformed dimensionless pressure in Laplace domain. Eq. 2.32 is the tempered fractional linear flow equation in Laplace space.

2.6 Constant Rate Inner Boundary and No-flow Outer Boundary Condition

Though dimensionless pressure is used in the equation, the definition of it is yet to be finished. Assume constant rate inner boundary condition, by the flux law shown in Eq. 2.2, the flow rate at the wellbore is:

$$\frac{k(L_f\,h)}{\mu B}\frac{\partial^{1-\alpha}}{\partial t^{1-\alpha}}\left[\frac{\partial}{\partial x}p(x,t)\right]_{x=0} = q_w \quad (2.33)$$

where L_f is the half length of the fracture we considered in this study. Thus, the area of the fracture wing is

$$A_f = L_f h \quad \text{.....(2.34)}$$

Since the penetration ratio is set to one as mentioned above and combine the definition of characteristic length, L shown in Eq. 2.20, the area of the fracture wing shown in Eq. 2.34 can be expressed as

$$A_f = y_e h = L\sqrt{Ar}h \quad \text{.....(2.35)}$$

Substituting Eq. 2.35 into the well flow rate equation shown in Eq. 2.33, we can obtain

$$\frac{k\left(L\sqrt{Ar}h\right)}{\mu B}\frac{\partial^{1-\alpha}}{\partial t^{1-\alpha}}\left[\frac{\partial}{\partial x}p(x,t)\right]_{x=0} = q_w \quad \text{.....(2.36)}$$

Rearrange Eq. 2.36 to

$$\frac{k(Lh)}{\mu B}\frac{\partial^{1-\alpha}}{\partial t^{1-\alpha}}\left[\frac{\partial}{\partial x}p(x,t)\right]_{x=0} = \frac{q_w}{\sqrt{Ar}} \quad \text{.....(2.37)}$$

Now we can define that the production rate based on drainage area is

$$q_A = \frac{q_w}{\sqrt{Ar}} \text{ or } q_w = q_A\sqrt{Ar} \quad \text{.....(2.38)}$$

Apply the definition of dimensionless distance (Eq. 17) and dimensionless pressure (Eq. 26) to Eq. 37, and get

$$\frac{k(Lh)}{\mu B}\frac{\partial^{1-\alpha}}{\partial t^{1-\alpha}}\left[\frac{\partial}{\partial L\, x_D}(p_i - p_{ch}p_D)\right]_{x_D=0} = q_A \quad \text{.....(2.39)}$$

Rearrange Eq. 19, by moving all terms other than derivative term to the right-hand-side, and we can get

$$\frac{\partial^{1-\alpha}}{\partial t^{1-\alpha}}\left[\frac{\partial}{\partial x_D}p_D\right]_{x_D=0} = \frac{q_A B\mu}{k(L\,h)}\left(\frac{L}{-p_{ch}}\right). \quad (2.40)$$

Now, for constant rate inner boundary condition, characteristic pressure can be defined as

$$p_{ch} = \frac{q_A B\mu\, L}{k(L\,h)} = \frac{q_A B\mu}{k\,h}. \quad (2.41)$$

Thus, the dimensionless pressure could be defined as

$$p_D = \frac{k\,h}{q_A B\mu}(p_i - p) \quad (2.42)$$

By defining the dimensionless pressure, we can then determine the constant rate inner boundary condition (Eq. 2.40) in dimensionless form as

$$\frac{\partial^{1-\alpha}}{\partial t^{1-\alpha}}\left[\frac{\partial}{\partial x_D}p_D\right]_{x_D=0} = -1 \quad (2.43)$$

Take Laplace transform with respect to time on Eq. 2.42, the transformed constant rate inner boundary condition becomes

$$\left[\frac{\partial}{\partial x_D}\left(\frac{s}{s^{\alpha}}\,\bar{p}_D\right)\right]_{x_D=0} = -\frac{1}{s}. \quad (2.44)$$

For convenience in solving equation set, we rearrange Eq. 2.44 by moving complex variable in Laplace domain, s and fractional derivative parameter, α to the right-hand-side of the equation that

$$\left[\frac{\partial}{\partial x_D}\bar{p}_D\right]_{x_D=0} = -\frac{1}{s^{2-\alpha}} \quad (2.45)$$

If taking Laplace transform to Eq. 2.43 with tempering factor, the transformed constant rate inner boundary condition becomes

$$\left[\frac{\partial}{\partial x_D}\left(\frac{s}{(s+\lambda)^{\alpha}-\lambda^{\alpha}}\bar{p}_D\right)\right]_{x_D=0}=-\frac{1}{s}. \quad (2.46)$$

The outer boundary condition is assumed to be no flow here, thus

$$\frac{\partial^{1-\alpha}}{\partial t^{1-\alpha}}\left[\frac{\partial}{\partial x_D}p_D\right]_{x_{eD}}=0 \quad (2.47)$$

where $x_{eD}=\frac{1}{\sqrt{Ar}}$.

Take Laplace transform of Eq. 2.47 with respect to time, we can get

$$\left[\frac{\partial}{\partial x_D}\left(\frac{s}{s^{\alpha}}\,\bar{p}_D\right)\right]_{x_{eD}}=0, \quad (2.48)$$

which can be reduced to

$$\left[\frac{\partial}{\partial x_D}\bar{p}_D\right]_{x_{eD}}=0. \quad (2.49)$$

If tempering factor is included, the no-flow outer boundary condition becomes

$$\left[\frac{\partial}{\partial x_D}\left(\frac{s}{(s+\lambda)^{\alpha}-\lambda^{\alpha}}\bar{p}_D\right)\right]_{x_D=x_{De}}=0 \quad (2.50)$$

Clearly, Eq. 2.50 can be reduced to Eq. 2.49 as well. So tempering factor will not make a difference on no-flow outer boundary condition.

Now, we can sum up the equation sets we need to use for constant rate inner boundary condition and no-flow outer boundary condition in dimensionless form and Laplace space with tempering factor:

$$\frac{\partial}{\partial x_D}\left[\frac{\partial}{\partial x_D}\left(\frac{s}{(s+\lambda)^{\alpha}-\lambda^{\alpha}}\bar{p}_D\right)\right]=s\,\bar{p}_D \quad (2.32)$$

Inner boundary: $\left[\frac{\partial}{\partial x_D}\left(\frac{s}{(s+\lambda)^{\alpha}-\lambda^{\alpha}}\bar{p}_D\right)\right]_{x_D=0}=-\frac{1}{s}$. (2.46)

Outer boundary: $\left[\frac{\partial}{\partial x_D}\bar{p}_D\right]_{x_{eD}}=0$ (2.49)

2.7 Constant Pressure Inner Boundary and No-flow Outer Boundary Condition

For constant pressure inner boundary condition, the pressure inside the fracture ($t_D=0$) does not change. Thus, for this kind of boundary condition, we can define characteristic pressure as the difference between initial reservoir pressure and well bottom-hole pressure that

$$p_{ch}=p_i-p_w. \quad (2.51)$$

Recall the definition of dimensionless pressure in Eq. 2.26, we can define the dimensionless pressure for constant pressure inner boundary condition as

$$p_D=\frac{p_i-p(x,t)}{p_i-p_w} \quad (2.52)$$

Hence, we can express constant pressure inner boundary condition as

$$p_D|_{x_D=0} = \frac{p_i - p(0,t)}{p_i - p_w} = 1 \quad \text{.....(2.53)}$$

Take Laplace transform with respect to time on Eq. 2.53, and get

$$\bar{p}_D|_{x_D=0} = \frac{1}{s} \quad \text{.....(2.54)}$$

If tempering factor is not considered, we can use Eq. 2.54 as the inner boundary condition, Eq. 2.49 as the outer boundary condition, and diffusivity equation (Eq. 2.31), to solve the problem. However, we still need to determine the dimensionless rate. Thus, we need to recall the flux law shown in Eq. 2.39:

$$\frac{k(Lh)}{\mu B}\frac{\partial^{1-\alpha}}{\partial t^{1-\alpha}}\left[\frac{\partial}{\partial L\, x_D}(p_i - p_{ch}p_D)\right]_{x_D=0} = q_A \quad \text{.....(2.39)}$$

Apply the definition of dimensionless pressure (Eq. 2.52) to Eq. 2.39, we can get

$$-(p_i - p_w)\frac{kh}{\mu B}\frac{\partial^{1-\alpha}}{\partial t^{1-\alpha}}\left[\frac{\partial}{\partial x_D}p_D\right]_{x_D=0} = q_A \quad \text{.....(2.55)}$$

Rearranging Eq. 2.55 by moving all the remaining parameters to the right-hand side to the equation that,

$$\frac{\partial^{1-\alpha}}{\partial t^{1-\alpha}}\left[\frac{\partial}{\partial x_D}p_D\right]_{x_D=0} = -\frac{1}{(p_i - p_w)}\frac{\mu B}{kh}q_A \quad \text{.....(2.56)}$$

Now, we can define the dimensionless production rate based on drainage area from the right-hand-side of Eq. 2.56 as

$$q_{AD} = \frac{1}{(p_i - p_w)} \frac{\mu B}{kh} \, q_A \quad \text{.....(2.57)}$$

Combing the definition of flow rate based on drainage area, dimensionless production rate based on Eq. 2.57 becomes

$$q_{wD} = \sqrt{Ar} q_{AD} = \frac{1}{(p_i - p_w)} \frac{\mu B}{kh} \, \sqrt{Ar} q_A \quad \text{.....(2.58)}$$

By applying the dimensionless flow rate (Eq. 2.58) to Eq. 2.56, we will get

$$\frac{\partial^{1-\alpha}}{\partial t^{1-\alpha}} \left[\frac{\partial p_D}{\partial x_D}\right]_{x_D=0} = -q_{AD}(t) \quad \text{.....(2.59)}$$

Without including the tempering factor, we can take Laplace transform with respect to time on Eq. 2.59 and get

$$\left[\frac{\partial \bar{p}_D}{\partial x_D} \frac{s}{s^\alpha}\right]_{x_D=0} = -\bar{q}_{AD} \quad \text{.....(2.60)}$$

Thus, in Laplace space, the dimensionless rate at the source is

$$\bar{q}_{wD} = -\sqrt{Ar} \left[\frac{\partial}{\partial x_D} \left(\frac{s}{s^\alpha} \bar{p}_D\right)\right]_{x_D=0} \quad \text{.....(2.61)}$$

In general, at any x_D location the flow rate is:

$$\bar{q}_D = -\sqrt{Ar} \frac{\partial}{\partial x_D} \left(\frac{s}{s^\alpha} \bar{p}_D\right) \quad \text{.....(2.62)}$$

In our model, we need to perform tempered fractional derivative, thus taking Laplace transform on Eq. 2.59 with respect to time will lead to

$$\left[\frac{\partial}{\partial x_D}\left(\frac{s}{(s+\lambda)^{\alpha}-\lambda^{\alpha}}\bar{p}_D\right)\right]_{x_D=0} = -\bar{q}_{AD} \quad \text{.....(2.63)}$$

Thus, we can obtain the flow rate at the source can be expressed as

$$\bar{q}_{wD} = -\sqrt{Ar}\left[\frac{\partial}{\partial x_D}\left(\frac{s}{(s+\lambda)^{\alpha}-\lambda^{\alpha}}\bar{p}_D\right)\right]_{x_D=0} \quad \text{.....(2.64)}$$

In general, at any x_D location the flow rate is:

$$\bar{q}_D = -\sqrt{Ar}\frac{\partial}{\partial x_D}\left(\frac{s}{(s+\lambda)^{\alpha}-\lambda^{\alpha}}\bar{p}_D\right) \quad \text{.....(2.65)}$$

Sum up constant pressure inner boundary condition and no flow outer boundary condition with tempering factor:

$$\frac{\partial}{\partial x_D}\left[\frac{\partial}{\partial x_D}\left(\frac{s}{(s+\lambda)^{\alpha}-\lambda^{\alpha}}\bar{p}_D\right)\right] = s\,\bar{p}_D \quad \text{.....(2.32)}$$

Inner boundary: $\bar{p}_D|_{x_D=0} = \frac{1}{s}$ .....(2.54)

Outer boundary: $\left[\frac{\partial}{\partial x_D}\bar{p}_D\right]_{x_{eD}} = 0$ .....(2.49)

Production rate: $\bar{q}_{wD} = -\sqrt{Ar}\left[\frac{\partial}{\partial x_D}\left(\frac{s}{(s+\lambda)^{\alpha}-\lambda^{\alpha}}\bar{p}_D\right)\right]_{x_D=0}$ .....(2.64)

2.8 Add Skin Factor

Firstly, we only show the derivation of adding skin factor to constant pressure inner boundary condition because constant pressure inner boundary condition is more practical

when comparing type curves to field data. Without considering the skin factor, recall the constant pressure inner boundary condition introduced in section 2.5 is

$$p_D|_{x_D=0} = \frac{p_i - p(0,t)}{p_i - p_w} = 1 \quad (2.53)$$

If there is low permeability zone around the fracture, or other conditions, there will be a difference between well pressure and reservoir pressure at $x_D = 0$. Thus,

$$p_D|_{x_D=0} = \frac{p_i - p(0,t)}{p_i - p_w} \neq 1 \quad (2.66)$$

If there is damage and positive skin factor, then

$p(0,t) > p_w$ and $p_i - p(0,t) < p_i - p_w$.

Now, we can define a pressure difference between the pressure inside the fracture and the pressure at the fracture face. This pressure difference is caused by a low permeability zone at the fracture face. In some literature, this effect is defined as fracture-face skin effect.

$$\Delta p_{skin} = p(0,t) - p_w \quad (2.67)$$

Eq. 2.67 can be arranged to

$$p(0,t) = p_w + \Delta p_{skin} \quad (2.68)$$

Substitute Eq. 2.68 into the dimensionless pressure definition in Eq. 2.66, we can get

$$p_D|_{x_D=0} = \frac{p_i - (p_w + \Delta p_{skin})}{p_i - p_w} = \frac{p_i - p_w}{p_i - p_w} - \frac{\Delta p_{skin}}{p_i - p_w} = 1 - \frac{\Delta p_{skin}}{p_i - p_w} \quad (2.69)$$

Since Δp_{skin} will be proportional to the current production rate whatever the production rate is, we can define that

$$\Delta p_{skin} = skin \times q_w \times Const1 \quad (2.70)$$

In Eq. 2.70, skin is the skin factor which is dimensionless; q_w is the production rate of the fracture; $Const1$ is a constant with the unit of pressure per rate, which is used to shift the unit of production rate to pressure difference caused by skin.

Recall the definition of dimensionless production rate and the solution of dimensionless production rate in Laplace Domain with tempering factor:

$$q_{wD} = \frac{1}{(p_i - p_w)} \frac{\mu B}{kh} q_w \quad (2.57)$$

$$\bar{q}_{wD} = -\sqrt{Ar} \left[\frac{\partial}{\partial x_D} \left(\frac{s}{(s+\lambda)^{\alpha} - \lambda^{\alpha}} \bar{p}_D \right) \right]_{x_D = 0} \quad (2.64)$$

Combine Eq. 57 and Eq. 64, we can find the solution of dimensional production rate in Laplace Domain with tempering factor is

$$\bar{q}_w = (p_i - p_w) \frac{kh}{\mu B} \bar{q}_{wD} = -(p_i - p_w) \frac{kh}{\mu B} \sqrt{Ar} \left[\frac{\partial}{\partial x_D} \left(\frac{s}{(s+\lambda)^{\alpha} - \lambda^{\alpha}} \bar{p}_D \right) \right]_{x_D = 0} \quad (2.71)$$

The unit of the constant that change dimensionless production rate to dimensional is

$$Const2 = (p_i - p_w) \frac{kh}{\mu B} = \frac{M}{LT^2} \times \frac{L^3}{\frac{M}{LT}} = \frac{L^3}{T} \quad (2.72)$$

which is the unit of the production rate. Thus $Const2$ represents the part of production rate in $Const1$.

Now, we can define another constant, $Const3$ which represents the unit of pressure in $Const1$ according to the dimensionless pressure definition in Eq. 5:

$$Const3 = (p_i - p_w) = \frac{M}{LT^2} \quad (2.73)$$

Thus, $Const1$ is defined as

$$Const1 = \frac{Const3}{Const2} = (p_i - p_w)\frac{1}{(p_i - p_w)}\frac{\mu B}{kh} = \frac{\mu B}{kh} = \frac{M}{LT^2} / \frac{L^3}{T} \quad (2.74)$$

Plug the definition of the constants back into Eq. 10, we can get

$$\Delta p_{skin} = skin \times q_w \times Const1 = skin\frac{Const3}{Const2}q_w = skin\frac{\mu B}{kh}q_w \quad (2.75)$$

The relationship between dimensional production rate and dimensionless production rate is

$$q_{wD} = \frac{1}{Const2}\, q_w \quad (2.76)$$

So for convenience, we can express the pressure difference caused by skin in terms of dimensionless production rate as

$$\Delta p_{skin} = skin\frac{Const3}{Const2}q_w = skin \times Const3 \times q_{wD} \quad (2.77)$$

Substitute Eq. 2.77 into Eq. 2.69, we can get

$$p_D|_{x_D=0} = 1 - \frac{skin \times Const3 \times q_{wD}}{p_i - p_w} \quad (2.78)$$

According to the definition of $Const3$ from Eq. 2.73, it will be cancelled. Arrange Eq. 2.78 and get

$$p_D|_{x_D=0} + skin \times q_{wD} = 1 \quad (2.79)$$

Laplace transform Eq. 2.79 with tempering factor, we can get

$$\bar{p}_D|_{x_D=0} + skin \times \bar{q}_{wD} = \frac{1}{s} \quad (2.80)$$

Substitute Eq. 2.64 into Eq. 2.80,

$$\bar{p}_D|_{x_D=0} - skin \times \sqrt{Ar} \left[\frac{\partial}{\partial x_D}\left(\frac{s}{(s+\lambda)^{\alpha}-\lambda^{\alpha}}\bar{p}_D\right)\right]_{x_D=0} = \frac{1}{s} \quad (2.81)$$

Eq. 2.81 is used as the constant pressure inner boundary condition with skin factor in our model.

2.9 Gaver Wynn's Rho (GWR) algorithm

The third step of this model is obtaining the solution of partial differential equations in Laplace domain with two types of inner boundary conditions. With tempered fractional derivative applied to linear flow regime, solving the equation set by hand is not practical and time consuming. In this case, we use Mathematica software to solve partial differential equations. After the solutions for dimensionless rate or dimensionless pressure is obtained in Laplace domain, there are two ways to obtain results in real time domain: analytical inversion and numerical inversion. For our model, with fractional parameter and tempering factor, the solution in Laplace domain is already complex. Thus, it is impossible to obtain the solution in real time domain analytically. So we choose to use Gaver Wynn's Rho algorithm to obtain solution in real time space (Valko and Abate, 2004). The basis of solving numerical inversion of Laplace transform problem is Gaver function, which is proved to be one of the most powerful methods (Valko and Abate, 2004).

Gaver functional:

$$f_\eta(t) = (-1)^\eta \tau\eta \binom{2\eta}{\eta} \Delta^\eta \hat{f}(\eta\tau) = \eta\tau \binom{2\eta}{\eta} \sum_{j=0}^{\eta} (-1)^j \binom{\eta}{j} \hat{f}\big((\eta + j)\tau\big) \quad \text{.....(2.82)}$$

In Eq. 2.82, $\tau = \ln(2)/t$ and Δ is the forward difference operator. Based on Eq. 2.82, there are many algorithms like famous Stehfest algorithm (Stehfest, 1970). However, Stehfest algorithm is not computationally efficient. Thus, we need to use sequence acceleration for numerical Laplace inversion. We have many choices for sequence acceleration including Neville's algorithm, Aitken's deta-square formula, Salzer summation, and so on. Valko and Abate (2004) compared five different sequence acceleration algorithms. Also, combing results from other literature, we find that Wynn's rho algorithm is effective and reliable (Osada, 1990; Cain and Berman, 2009).

The Wynn's rho Algorithm is then shown as (Wimp 1981)

$$\rho_{-1}^{(n)} = 0, \ \rho_0^{(n)} = f_n(t) \quad \text{when } n \geq 0 \quad \text{.....(2.83)}$$

$$\rho_k^{(n)} = \rho_{k-2}^{(n+1)} + \frac{a}{\rho_{a-1}^{(n+1)} - \rho_{a-1}^{(n)}} \quad \text{when } k \geq 1 \quad \text{.....(2.84)}$$

with the additional caveat that $f_n(t)$ in equation (2.83) is calculated from equation (2.82) with η=n+1.

The approximant of the inverse at time *t* is then $f(t, 2m) = \rho_{2m}^{(0)}$. We chose the GWR algorithm to perform numerical inversion of Laplace transform.

3. MODEL VERIFICATION

After the model is constructed, we use Mathematica software for differential equation sets, and then perform GWR numerical inversion to obtain results. We need to verify this model firstly with some published results. Firstly, we compare our model with numerical model to verify our basic model settings, assumptions, and dimensionless variable definitions are correct. The numerical model does not use sub-diffusion flow regime, so we set the fractional parameter, $\alpha = 1$ and tempering factor $\lambda = 0$. Furthermore, there is no model included tempering factor in the linear flow model of petroleum engineering research. Thus we choose to verify our model with fractional derivative model (Raghavan, 2011; Rhagavan, 2012; Rhagavan and Chen, 2013; Chen and Raghavan, 2015; Raghavan and Chen, 2017). To compare the validity of our model, we set the tempering factor, $\lambda = 0$ and compare the results obtained by Raghavan and Chen (2017).

3.1 Compare with Numerical Model

In order to compare our linear flow model with numerical model, we use a synthetic data set. Major input parameters of the numerical model is shown in Table 3.1 below. In the square reservoir model, a vertical well is placed in the center and this well has a bi-wing fracture which has fully penetrated this reservoir model and it is parallel to the side of the reservoir model. We use IMEX from CMG software, which is designed for black oil reservoir because our model assumed slightly compressible fluid. Furthermore, we set the

well to produce with constant bottom-hole pressure of 8000 psi. The initial reservoir pressure is assumed to be 8125 psi so the pressure change won't make the oil formation volume factor change dramatically.

Table 3.1 - Parameters input to numerical model.

Parameter	Value
Model length and width	420 ft × 420 ft
Model height	20 ft
Porosity	21%
Rock Permeability	0.001 md
Viscosity	0.175 cp
Initial oil formation factor	2.82 bbl/STB
Oil compressibility	$1.75 \times 10^{-5}\ psi^{-1}$
Rock compressibility	$3.0 \times 10^{-5}\ psi^{-1}$
Initial reservoir pressure	8125 psi
Well bottom-hole pressure	8000 psi

After the data computed by numerical model is output, we need to compute dimensionless variables based on production rate and time. Recall the dimensionless variables defined in methodology section:

Dimensionless flow rate based on drainage area: $q_{AD} = \frac{q_{wD}}{\sqrt{Ar}} = q_{DC} \frac{1}{(p_i - p_w)} \frac{\mu B}{kh} \frac{q_w}{\sqrt{Ar}}$.

Dimensionless time: ${t_D}^{\alpha} = t_{DC} \frac{k}{\phi \mu c L^2} t^{\alpha}$.

The parameters use to calculate these two dimensionless variables are all shown in Table 3.1. However, these parameters are in field units, so while calculating dimensionless flow rate and time, we need to multiply by constants, q_{DC} and t_{DC}. The unit of time we used is

in day. Thus, in order to compute dimensionless time, $t_{DC} = 6.3283 \times 10^{-3}$. The production rate is in STB/day so $q_{DC} = 887.24$. There is another point we need to mention while calculating dimensionless flow rate and dimensionless time that as shown in Fig. 2.1, our model is a quarter region linear flow model of a single fracture. Thus, the flow rate q_w needs to be divided by four. Moreover, the length and width need to be divided by two to calculate characteristic length that $L = \sqrt{210\ ft\ \times 210\ ft} = 210\ ft$.

The results is shown in Fig. 3.1 below. We can see that our model matches numerical model well both in short term and long term. There is small deviation after reaching boundary dominated flow but not severe.

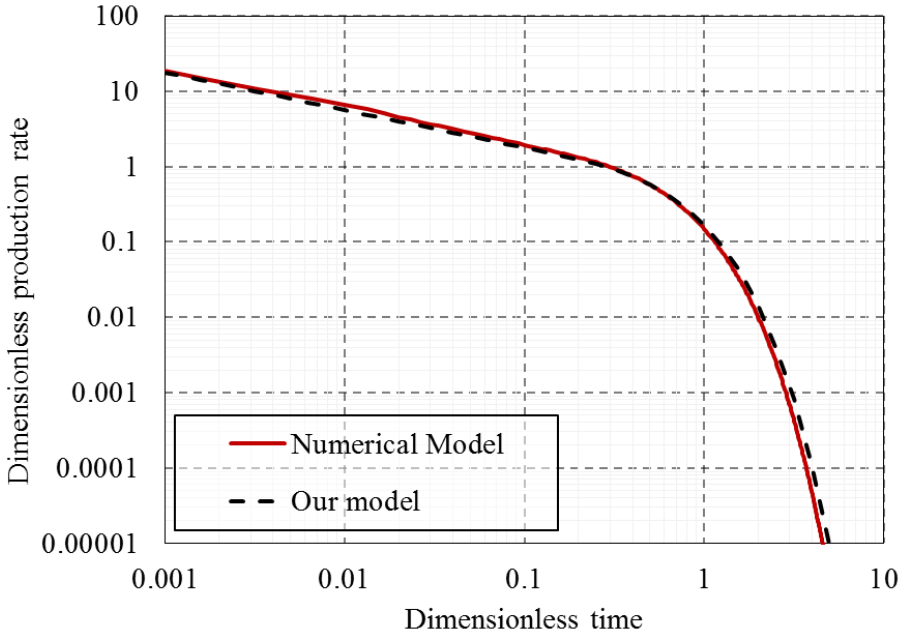

Figure 3.1 - Comparison of our model with numerical model of short term and long term data.

In Fig. 3.1, the transient period is not clear, so we choose to zoom-in and have a close look on the transient period, which is shown in Fig. 3.2 below. We can notice that the line of numerical model is not a perfect straight line and it slightly deviates from the line of our model. There are many factors may cause this observation because the numerical model has more input parameters than our model. The numerical model has discretized blocks that may affect the result as well.

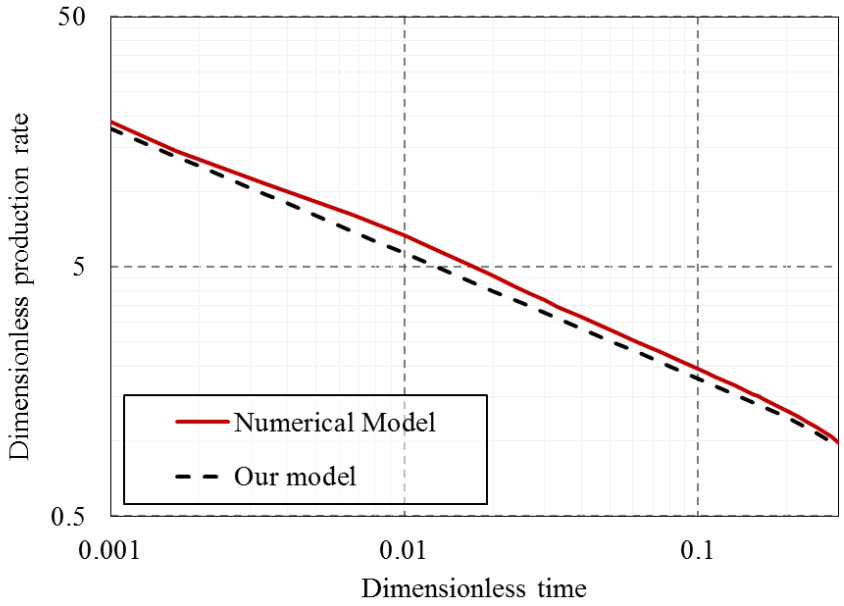

Figure 3.2 - Comparison of our model with numerical model in transient period.

3.2 Compare with Fractional Derivative Model

In this part, we compare the type curves of our model with Rhagavan and Chen's (2017) fractional derivative linear flow model. There are some differences in the definition of dimensionless variables so we need to consider that while comparing the results. The first one if the definition of characteristic length. In Eq. 2.20, we defined that the characteristic

length, $L = \sqrt{x_e\, y_e}$. However, characteristic length is defined as fracture half-length, L_f by Raghavan and Chen (2017). Secondly, the dimensionless pressure defined by Raghavan and Chen (2017) is multiplied by a 2π term while our definition of dimensionless pressure in Eq. 2.26 does not include this term. Similarly, the dimensionless flow rate defined by Raghavan and Chen (2017) is divided by a 2π term while our definition of dimensionless flow rate does not. Incorporating all these differences, we can compare our result with Raghavan and Chen's (2017) results.

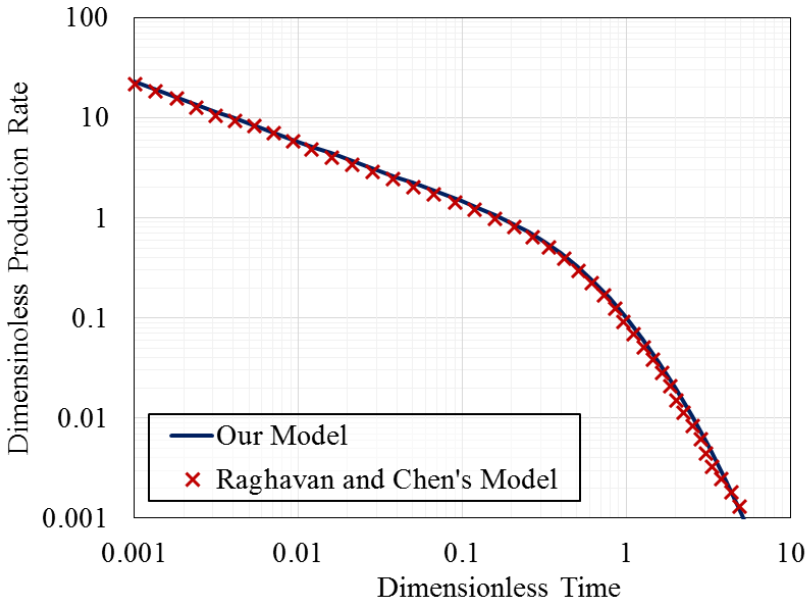

Figure 3.3 - Comparison of our model with Raghavan and Chen's (2017) model with constant pressure inner boundary condition (square drainage region and fractional parameter alpha = 0.9).

Raghavan and Chen (2017) show the result of their fractional derivative linear flow model with both constant pressure and constant rate inner boundary condition. Fractional

parameter alpha is set to 0.9, and the fracture fully penetrates the drainage area in the center of the drainage area. Raghavan and Chen's model (2017) incorporate dimensionless fracture conductivity so it is bi-linear flow model compared to our linear formation flow model. However, Raghavan and Chen show the result of their model with dimensionless fracture conductivity (definition shown in Eq. 2.13) of 1000, which is high enough compared to our assumption of infinite fracture conductivity. In Fig. 3.3 above, the result of constant pressure inner boundary condition is shown. We can observe that the result from our model matches the result from Raghavan and Chen's (2017) result under constant pressure inner boundary condition for both short term before pressure transient reaching drainage boundary, and long term of boundary dominated condition. For constant rate inner boundary condition, the results is shown in Fig. 3.4 below. We can observe in Fig. 3.4 that our model's result is same as the result from Raghavan and Chen's model (2017) for both short term and long term. Both Fig. 3.3 and 3.4 show that our tempered fractional derivative linear flow model is valid while we set tempering factor to zero. After our model's validity is verified, we can then use it to generate type curves, and use these type curves to study sub-diffusion behavior in field data.

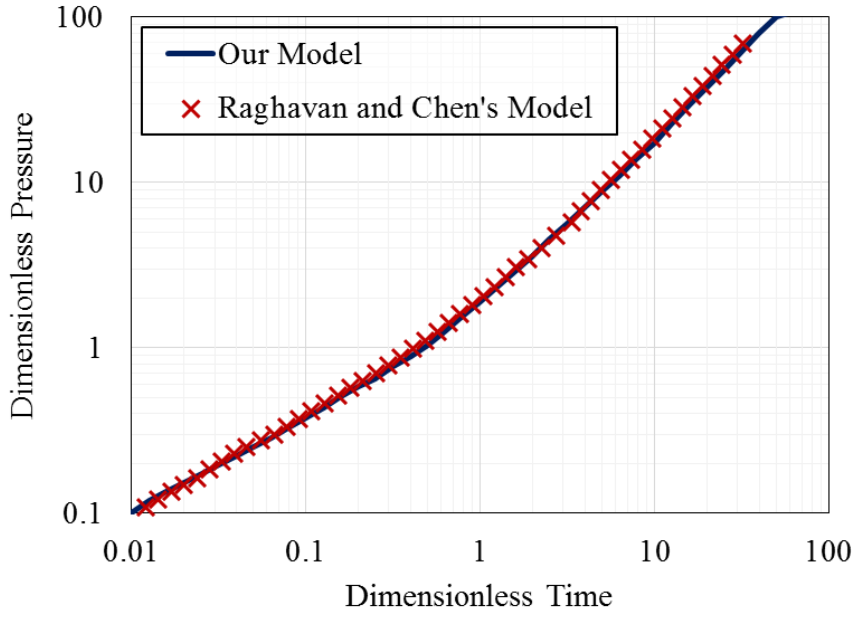

Figure 3.4 - Comparison of our model with Raghavan and Chen's (2017) model with constant rate inner boundary condition (square drainage region and fractional parameter alpha = 0.9).

4. RESULTS AND DISCUSSION

In this section, we use our model to generate type curves with different fractional parameter, tempering factor, skin factor, and aspect ratio. We discussed two types of inner boundary conditions for the model including constant rate and constant pressure inner boundary condition. However, constant rate inner boundary condition is less useful compared to constant pressure inner boundary condition. The reason is that for field production, some wells keep producing at a constant or slightly vibrating bottom-hole pressure for a long term, but we cannot find wells that keep producing at a constant rate for a long term. Thus, in this section, we focus on discussing the type curves of constant pressure inner boundary condition.

Before generating type curve plots, we show the solution of our model in Laplace domain. For constant pressure inner boundary condition, the solution of dimensionless pressure in Laplace domain is too complicated. So we choose to show the solution of dimensionless flow rate at inner boundary in Laplace domain by the definition shown in Eq. 2.64 as

$$\bar{q}_{wD} = \left(s \times skin + \frac{coth\left(\frac{\sqrt{(s+\lambda)^{\alpha}-\lambda^{\alpha}}}{\sqrt{Ar}}\right)\sqrt{(s+\lambda)^{\alpha}-\lambda^{\alpha}}}{\sqrt{Ar}} \right)^{-1} \quad \text{.....(4.1)}$$

We can obtain some special solutions based on Eq. 4.1 that if skin factor is 0 then

$$\bar{q}_{wD} = \frac{\sqrt{Ar}\times tanh\left(\frac{\sqrt{(s+\lambda)^{\alpha}-\lambda^{\alpha}}}{\sqrt{Ar}}\right)}{\sqrt{(s+\lambda)^{\alpha}-\lambda^{\alpha}}} \quad \text{.....(4.2)}$$

Furthermore, if skin factor and tempering factor are both 0, then

$$\bar{q}_{wD} = \frac{\sqrt{Ar} \times tanh\left(\sqrt{\frac{s^{\alpha}}{Ar}}\right)}{\sqrt{s^{\alpha}}} \quad (4.3)$$

The simplest case will be $Ar = 1$, $\alpha = 0$, $\lambda = 0$, and $skin = 0$. The solution of this special case becomes

$$\bar{q}_{wD} = \frac{tanh\left(\sqrt{\frac{s}{Ar}}\right)}{\sqrt{s}} \quad (4.4)$$

After obtaining the solution of dimensionless flow rate in Laplace domain, we also need to obtain the solution of dimensionless cumulative production. The dimensionless cumulative production is the integration of dimensionless flow rate at inner boundary condition. Thus, in Laplace domain, we can show that

$$\bar{Q}_{wD} = \frac{\bar{q}_{wD}}{s} \quad (4.5)$$

After solving for Eq. 4.5 in Laplace domain, we can get

$$\bar{Q}_{wD} = \left[s \left(s \times skin + \frac{coth\left(\frac{\sqrt{(s+\lambda)^{\alpha} - \lambda^{\alpha}}}{\sqrt{Ar}}\right)\sqrt{(s+\lambda)^{\alpha} - \lambda^{\alpha}}}{\sqrt{Ar}} \right) \right]^{-1} \quad (4.6)$$

In order to understand the behavior of sub-diffusion behavior, only dimensionless production rate and cumulative production are not enough. So after numerically inverting

the solution to real time domain using GWR algorithm (Section 2.8), we choose to calculate productivity index to comprehensively show the behavior of tempered fractional derivative linear flow model. There are different definitions of dimensionless productivity index from literature (Raghavan, 1993; Wattenbarger et al., 1998; Diyashev and Economides, 2006)). We define dimensionless productivity index as

$$J_D = \frac{q_{wD}}{\pi\left(1-Q_{wD}\sqrt{Ar}\right)} \quad \text{.....(4.7)}$$

4.1 Effect of Fractional Parameter

Firstly, we discuss the effect of fractional parameter. In this case, we set the tempering factor to be $\lambda = 0$, no skin effect, and square drainage region which means $Ar = 1$. Thus, we can clearly see the effect of fractional parameter α. The result of dimensionless production rate versus dimensionless time is shown in Fig. 4.1 below. We can observe that the zero case which express classical diffusion, shows exponential decline in rate at boundary dominated long term. However, with fractional parameter smaller than one, we can see the curves of dimensionless production rate show power-law decline rate at long term as mentioned by Raghavan and Chen (2017). Also, as fractional parameter decreases, we can see that the decline rate of dimensionless production rate curves getting smaller at long term. The observations mentioned above are all expected before this research. However, we find that the fractional parameter also has affected the type curves of

dimensionless production rate in short term before the pressure transient reach the boundary of the drainage area. Fig 4.1 does not clearly show this observation, so we zoom in and show these curves in short term in Fig. 4.2 below.

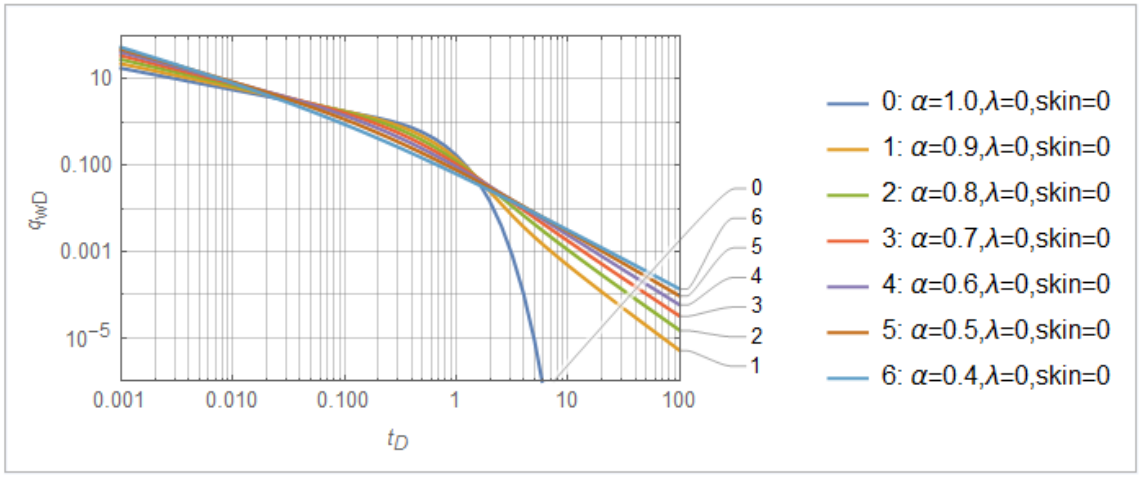

Figure 4.1 – Effect of fractional parameter on dimensionless production rate in short term and long term.

In Fig. 4.2, we observe that in short term, before pressure transient reach the boundary of the drainage area, smaller fractional parameter causes dimensionless production rate curves declines quicker in short term. We know that in short term, the dimensionless flow rate curves are straight lines on the log-log plot. So, smaller the fractional parameter, larger the slopes of dimensionless production rate curves will be. Also, while fractional parameters getting smaller, the dimensionless production rate curve will have larger intercept on y-axis. Previous research on fractional derivation linear flow model focuses

on the effect at boundary-dominated term. Our study shows that fractional diffusion may also has significant effect on short term transient flow.

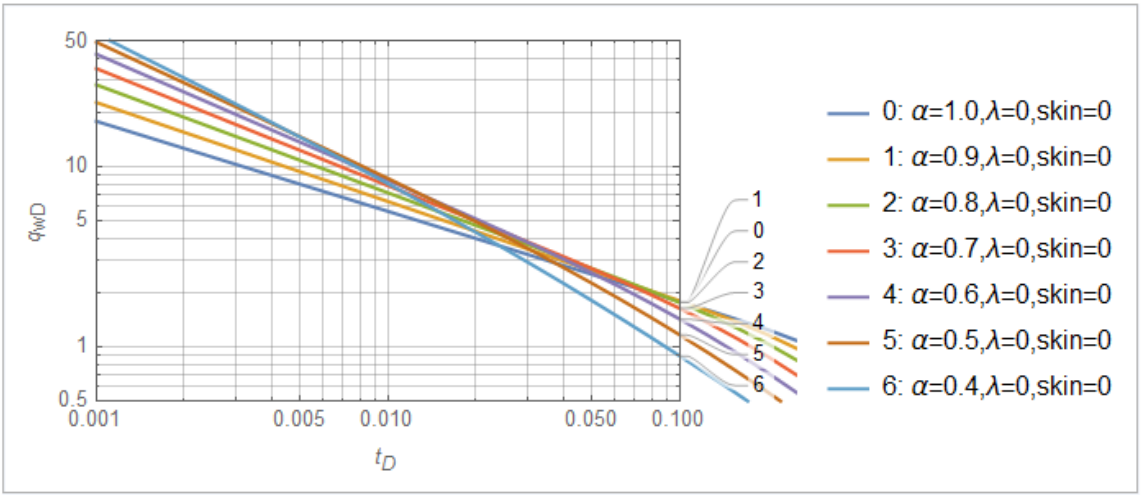

Figure 4.2 - Effect of fractional parameter on dimensionless production rate in short term.

In Fig. 4.3, we plot dimensionless cumulative production versus dimensionless time. Clearly, all the curves reaches one at long enough time. We need to mention that the dimensionless production reaches one does not mean the reserves are fully recovered. However, it means that under certain well bottom-hole pressure, all recoverable oil is produced. We observe that when fractional parameter becomes larger, the cumulative production curve increases slower and reaches one later.

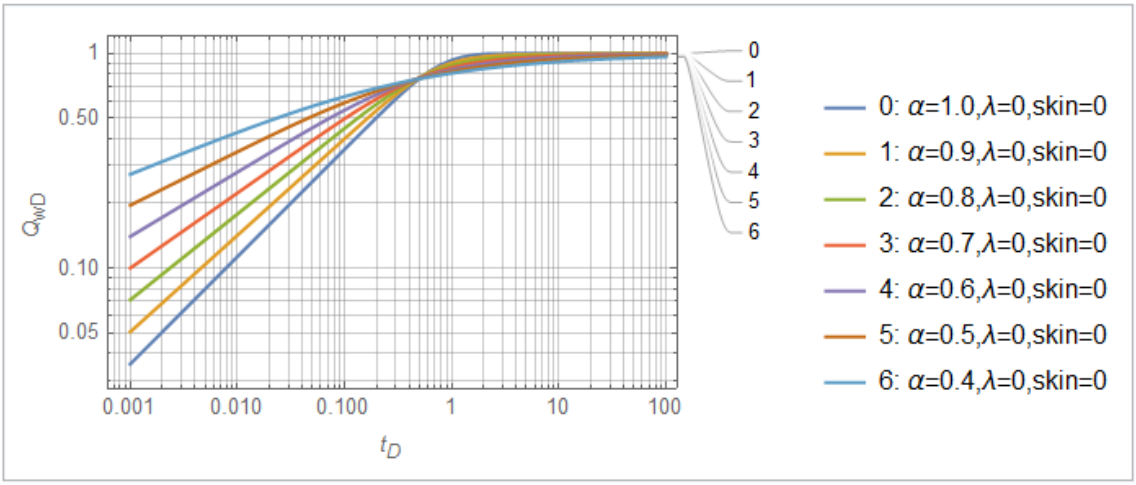

Figure 4.3 - Effect of fractional parameter on dimensionless cumulative production.

In Fig. 4.4, we plot dimensionless productivity index versus dimensionless time. Firstly, we observe that compared to out zero case, all fractional linear flow curves does not level off in long term. In short term before pressure transient reaching drainage area boundary, smaller fractional parameter results in faster decline rate. After reaching buondary-dominated condition, the curve of fractional parameter closer to one shows firstly a slower declining rate, but then drops faster again. For smaller fractional parameter, the curve of dimensionless productivity index is closer to a straight line, and does not change declining rate while pressure transient reaching drainage area boundary. Actually, when fractional paramete alpha equals 0.4 or 0.5, the curves of dimensionless productivity index are almost straight lines on the log-log plot. We can conclude that the dimensionless productivity index curve does not level off when fractional parameter is not one. We

concern that this observation may be not true for field data. Thus, we include tempering factor in our model and study its effect.

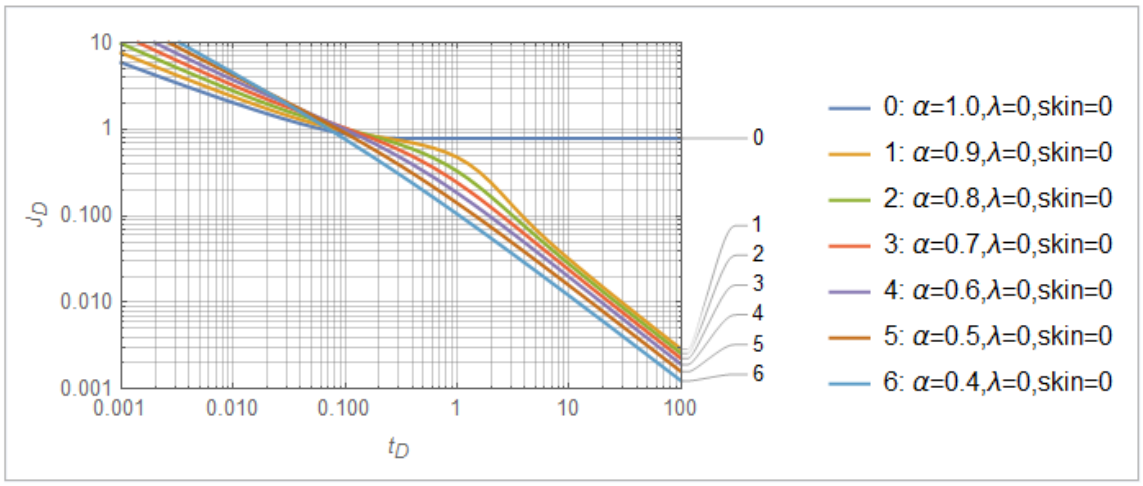

Figure 4.4 - Effect of fractional parameter on dimensionless productivity index.

4.2 Effect of Tempering Factor

In this section, we study the effect of tempering factor on traditional fractional derivative linear flow model. In order to study the effect of tempering factor, we control fractional parameter to be 0.8, and also, the zero case of classical diffusion is included in the figures for comparision. Since the tempering factor is novel in the study, we start from generating results with tempering factor in a wide range from 0.001 to 10 increasing by multiplying 10. Firstly, we plot dimensionless production rate versus dimensionless time in Fig. 4.5. In this plot, we can clearly see that the tempering factor successfully temper the power-law behavior of fractional linear flow in long-term boundary-dominated condition.

Actually, when tempering factor reaches ten, the curve of dimensionless production rate drops faster than zero case classical diffusion curve in long-term. In Fig. 4.5, we can see that while tempering factor increases, the dimensionless flow rate curve drops faster in long-term. When tempering factor is 0.001, the tempering phenomenon is not obvious, and the curve still shows power-law behavior in long-term. As tempering factor increases, the dimensionless production rate curve is tempered and gets closer to exponential behavior in long-term. From Fig. 4.5, we find that the most effective range of tempering factor for long-term could be between 0.1 and 1.0 so we will discuss the tempering factor in this range below. Other than these observations in long-term behavior, we can observe that the tempering factor also affect diffusion behavior in short-term before pressure transient reaching the drainage area boundary. The curves in Fig. 4.5 does not clearly show the behavior in short-term, so we zoom it in to study the effect of tempering facto in short-term.

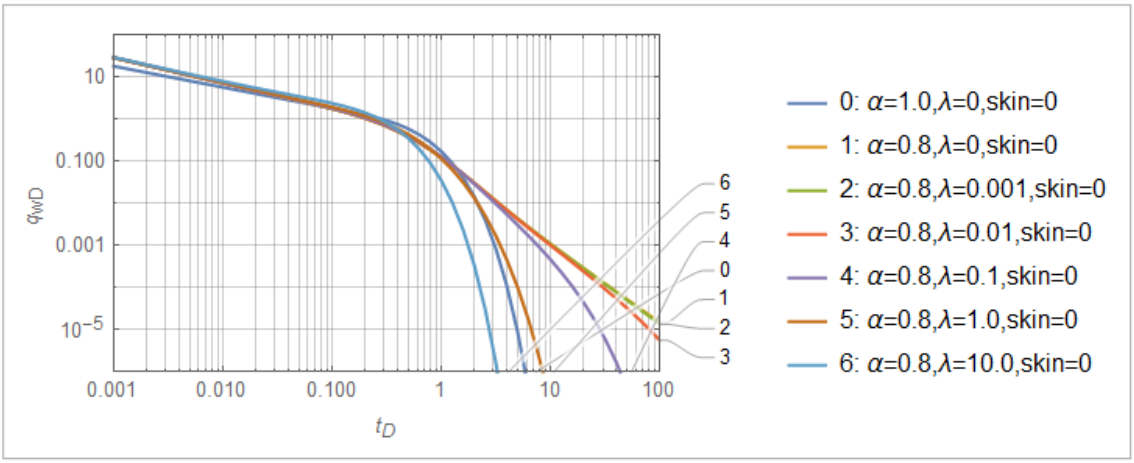

Figure 4.5 - Effect of tempering factor on dimensionless production rate in short term and long term.

In Fig. 4.6, we can observe the effect of tempering factor on dimensionless production rate in short-term. When fractional derivative is applied to linear flow regime, the main purpose is the effect on late-term. As discussed in section 4.1, we found the significant effect of fractional parameter on short-term behavior. In Fig. 4.6, we observe that the termpering factor has effect on short-term as well. When tempering factor is smaller than 0.1, the effect of tempering factor on short-term behavior is not significant. However, when tempering factor increases furthurly, we observe the decline slope of dimensionless production rate curve increases on log-log plot. When tempering factor reaches 10.0, the dimensionless production rate curve is parallel to the zero case of classical diffusion. Thus, for short-term, the most effective range of tempering factor is between 1.0 and 10.0, and we will study the tempering factor in this range below.

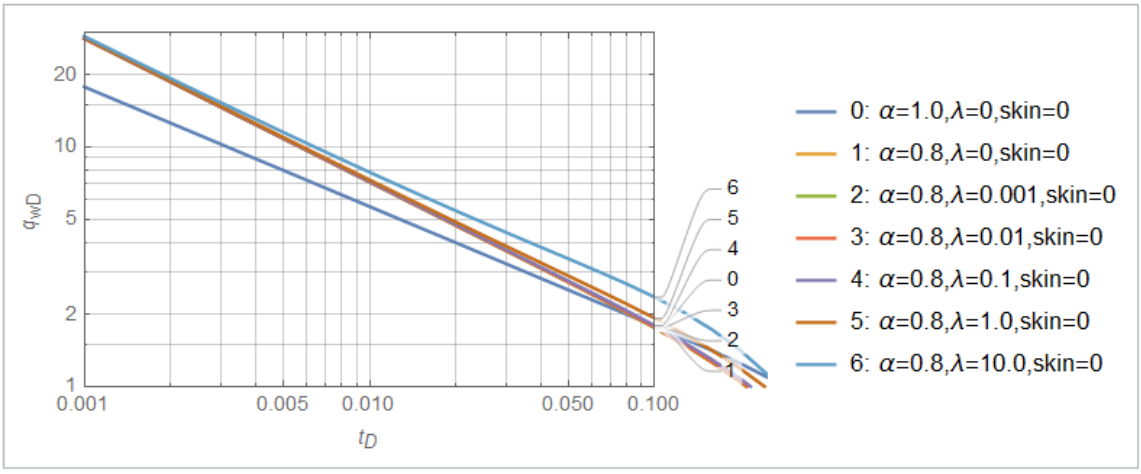

Figure 4.6 - Effect of tempering factor on dimensionless production rate in short term.

In Fig. 4.7, we plot dimensionless cumulative production versus diemnsionless time with different tempering factor. In section 4.1, we introduce that fractional parameter makes dimensionless cumulative production curve increases slower and reach one at a later time compared to classical diffusion zero case. From Fig. 4.7, we observe that dimensionless cumulative production curve has a larger slope with larger tempering factor. However, this relatioship is not obvious even when tempering factor equals one. While temperin factor reaches 10, the cumulative production curve has a larger slope and reaches 1.0 dimensionless cumulative production significantly ealier. This observation shows that though small tempering factor (smaller than 1) has only slight effect on dimensionless cumulative production, larger tempering factor does play an important tole in the model.

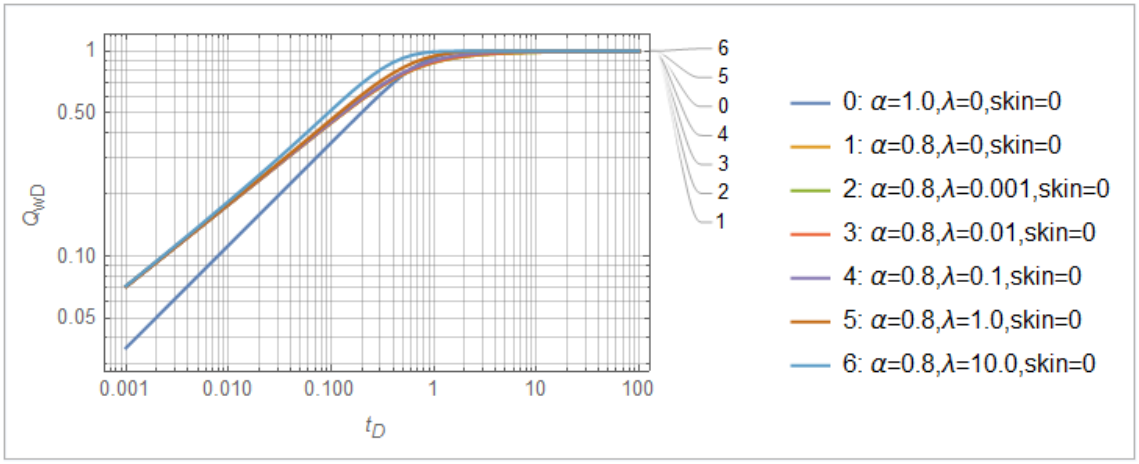

Figure 4.7 - Effect of tempering factor on dimensionless cumulative production.

The curves of dimensionless productivity index with different tempering factor is shown in Fig. 4.8. We observe that while tempering factor increases, the dimensionless productivity index curve declines at a smaller rate after reaching boundary dominated long

term. When tempering factor reaches 1.0, the dimensionless productivity index curve level off eventually. Furthermore, when tempering factor is 10.0, we can see the dimensionless productivity index curve levels off earlier and at a higher productivity index value. In a nutshell, compared to fractional derivative linear flow model, tempered fractional linear flow model lets dimensionless productivity index stabilize at long enough production period. Though wells may not produce long enough for dimensionless time to be bigger than 10, the observations mentioned above can still let us study sub-diffusion behavior.

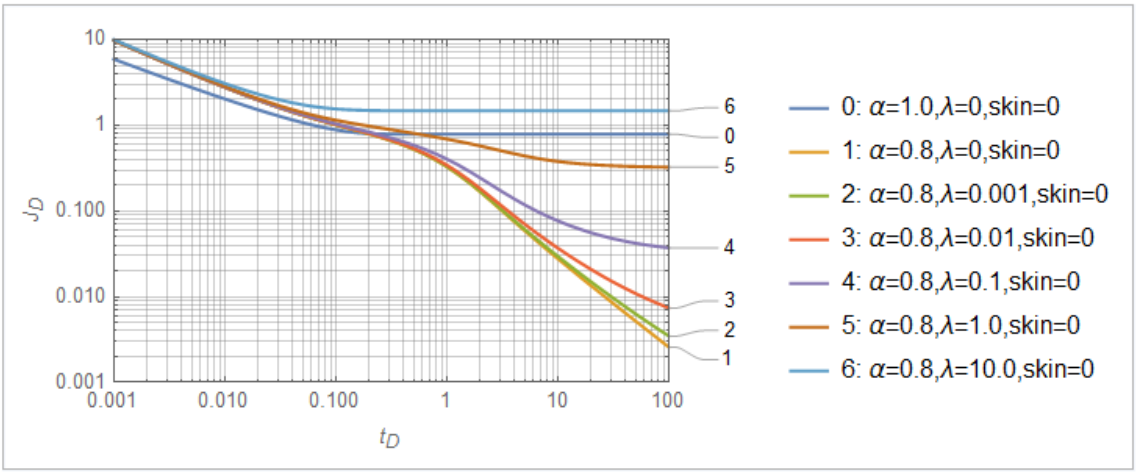

Figure 4.8 - Effect of tempering factor on dimensionless productivity index.

As mentioned above, we have two ranges of tempering factor to research on furtherly. Firstly, we generate type curves of tempering factor ranges from 0.2 to 1.0. In Fig. 4.9, we can clearly see that with tempering factor is between 0.2 and 1.0, the curves of dimensionless production rate have decline rate between classical diffusion zero case and

non-tempered fractional linear low of first case. Thus, this range of tempering factor is useful to model the sub-diffusion behavior which is not classical diffusion but has a faster declining rate of dimensionless flow rate compared to traditional fractional model. However, further research on the tempering factor should be performed after comparing to various field data set. The effect of tempering factor within this range (0.2 to 1.0) does not have significant effect on the declining rate of dimensionless production rate in short term.

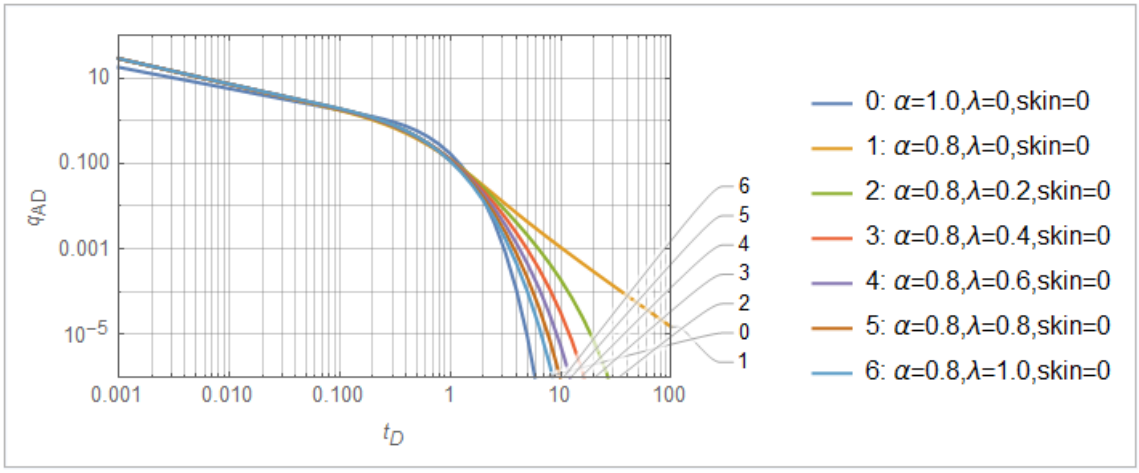

Figure 4.9 - Effect of tempering factor (from 0.2 to 1.0) on dimensionless production rate.

Another range of interest from previous study ranges from 1 to 10. In Fig. 4.10, we plot dimensionless production rate from 2 to 10. We can observe that the tempering factor within this range significantly affect the slope of dimensionless production rate curves in short term on log-log plot. In another word, tempering factor tempers the effect of

fractional derivative in short term before pressure transient reaching drainage area boundary.

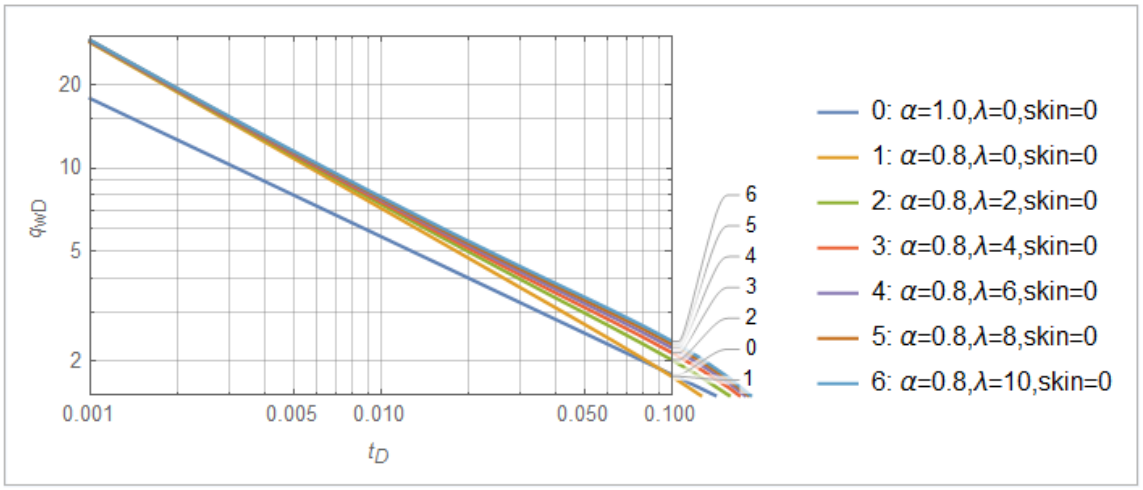

Figure 4.10 - Effect of tempering factor (from 2 to 10) on dimensionless production rate.

4.3 Effect of Skin Factor

As shown in section 2.7, we have included skin effect in our model. Skin effect can significant affect the production for unconventional reservoir. We expect even small skin factor will dramatically impact the result of our tempered fractional derivative linear flow model. Thus, we plot dimensionless production rate versus dimensionless time with skin factor ranging from 0 to 5 in Fig. 4.11. We keep fractional parameter and tempering factor constant in this section to be 0.8 and 0.4. While skin factor increases, the dimensionless production rate starts from a lower value, and drops slower. Also, the pressure transient

reaches drainage area boundary at a later time with increasing skin factor. The skin effect is not significant with 0.1 value, but for skin factor of 0.5, we can observe the production process is dramatically impacted. When skin factor is as high as 5, the dimensionless production rate curve keeps a low value in short term before boundary dominated condition. In fact, if operators encounter such condition in short term production, they may consider further treatment like re-fracturing or acidizing. In Fig. 4.12, the result of dimensionless cumulative production versus dimensionless time is shown. Fig. 4.12 furtherly demonstrate the effect of large skin factor to our model. While skin factor increases, the dimensionless cumulative production curve increases at a smaller slope and reaches value of one at a later time. For skin factor of 5, dimensionless cumulative production reaches one after dimensionless time of 10. These observations all reveal the significance of avoiding skin effect in unconventional reservoir which follow sub-diffusion behavior.

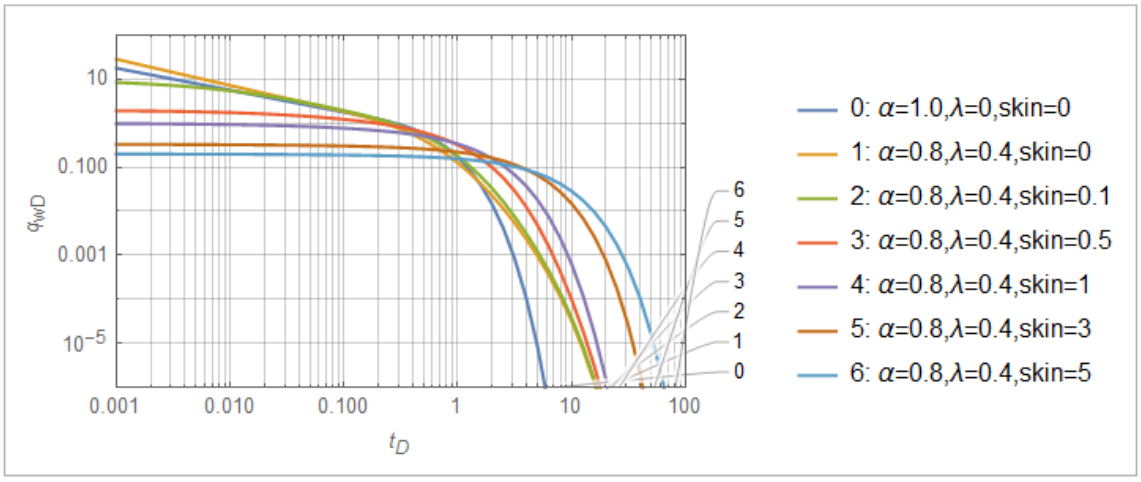

Figure 4.11 - Effect of skin factor on dimensionless production rate in short and long term.

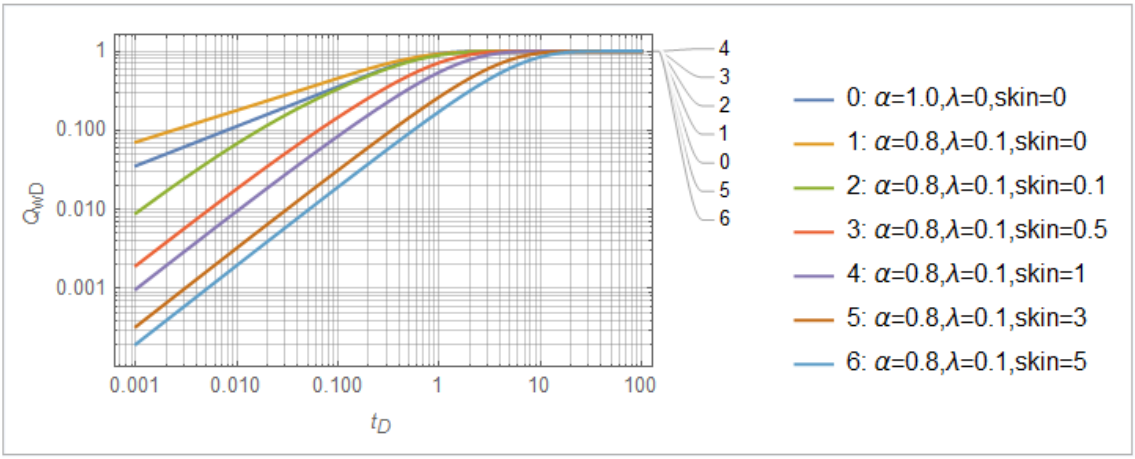

Figure 4.12 - Effect of skin factor on dimensionless cumulative production.

Moreover, we plot dimensionless productivity index versus dimensionless time with skin effect in Fig. 4.13. The impact of skin effect on production is shown more clearly. When skin factor is below 1.0, the curves of dimensionless productivity index still has similar pattern as non-skin curves but with low value and low declining rate. While skin factor reaches 3, dimensionless productivity index is extremely low in short term. Thus, the whole curve looks like a horizontal straight line with ultra-low value in all the terms of production on the log-log plot.

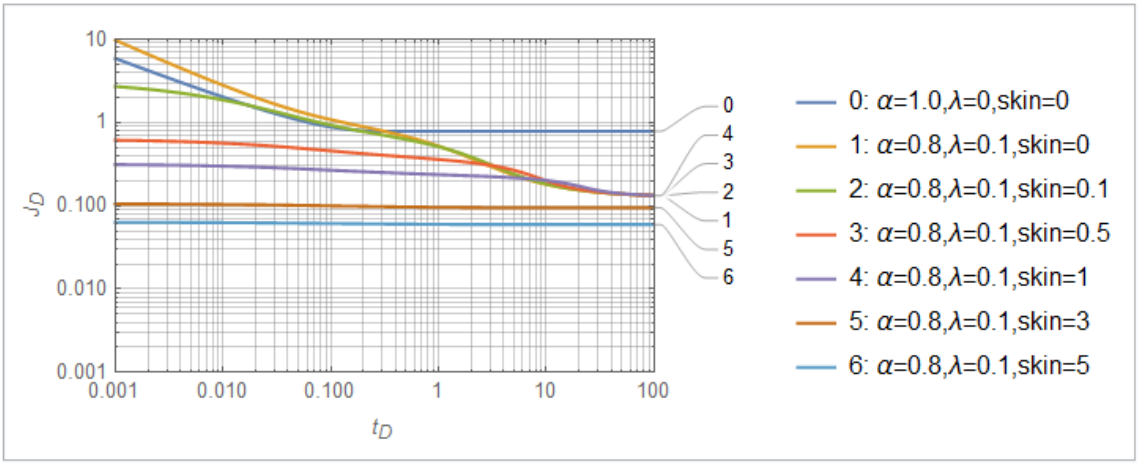

Figure 4.13 - Effect of skin factor on dimensionless productivity index.

4.4 Effect of Aspect Ratio of Rectangular Drainage Area

One of the merit of our model is that it incorporate aspect ratio. Rectangular drainage area is appropriate to model linear formation flow. However, operators may design fractures with different half-length and different fracture spacing. Thus, the ratio of length and width of the drainage area may be different. In this case, our model becomes suitable for more situations. In this section, we keep fractional parameter and tempering factor to be constant of 0.8 and 0.4. Also, no skin effect is considered in this section, In Fig. 4.14, we plot dimensionless production rate versus dimensionless time with aspect ratio from 0.25 to 2.00. Recall the definition of aspect ratio in section 2.5 that $Ar = y_e/x_e$. Clearly, when aspect ratio is smaller than 1.0 and the fracture fully penetrated the drainage area, the fracture length is shorter than the distance from the fracture to the outer boundary of the drainage area. Thus, larger aspect ratio may be considered as tighter fracture spacing and

vice versa. In Fig. 4.14 and Fig. 4.15, we observe that while aspect ratio increases, the dimensionless production rate curve reaches boundary-dominated condition at earlier time as expected. In short term before pressure transient reach drainage area boundary, the dimensionless production rate curves are have same slope on the log-log plot. Though these curves show same declining rate in short term, increasing aspect ratio still results in larger dimensionless production rate at same dimensionless time.

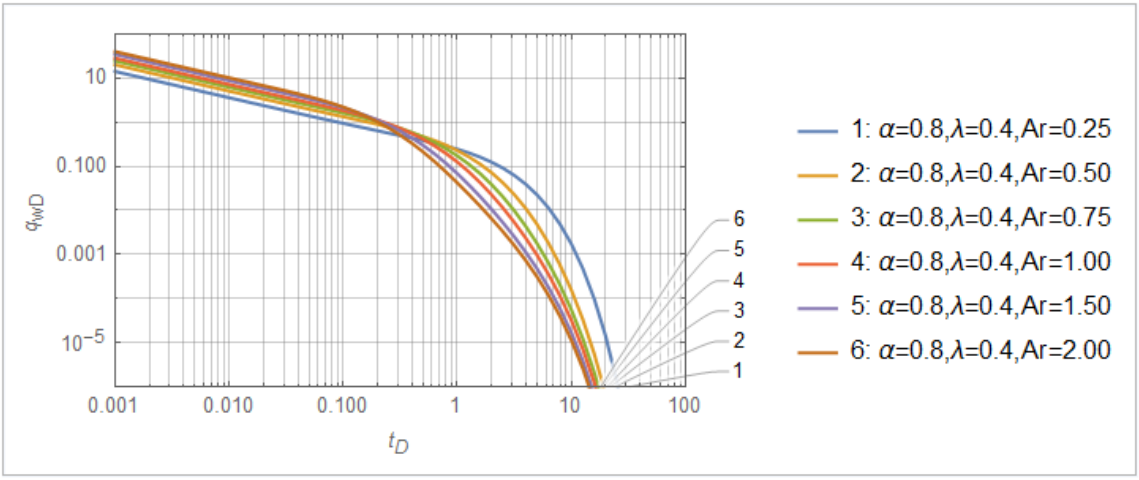

Figure - 4.14 Effect of aspect ratio on dimensionless production rate in short and long term (no skin).

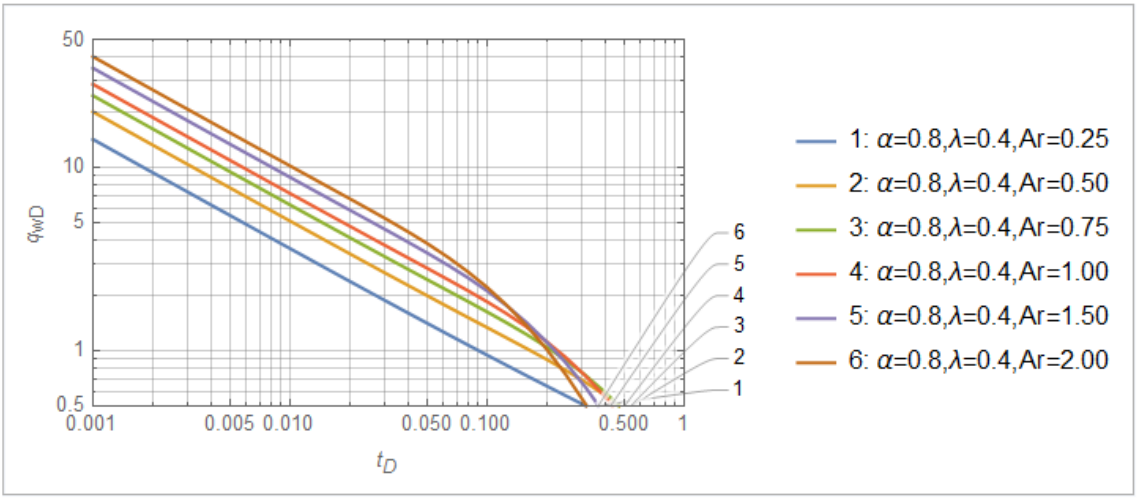

Figure - 4.15 Effect of aspect ratio on dimensionless production rate in short term (no skin).

4.5 Computational Time and Accuracy Check of GWR Inversion

We use GWR algorithm (introduced in section 2.8) to numerically invert results from Laplace domain back in real time domain. Thus, accuracy check and computational time are two issues we need to discuss here. One of the merit of GWR inversion is that we can adjust the necessary n-terms to obtain high precision results. In our tempered fractional derivative model, different fractional parameter or tempering factor may require different n-terms of GWR inversion in order to obtain accurate results. In the meantime, more terms of GWR inversion means longer computational time. So we perform accuracy check and choose the least terms that will yield accurate results to save computational time.

In Table 4.1, we show part of the dimensionless production rate of α=0.8 and λ=0.1 with increasing n-terms of GWR inversion from 8 to 512. We can see that after dimensionless

time reaches 10, the dimensionless production rate value becomes extremely small. When we use 16 n-terms, the solution is already stable. We only show three digits after decimal point in Table 4.1, so we show the percentage of difference between results from adjacent n-terms in Table 4.2. For example, in Table 4.2 the result of 16-term column is the difference percentage between 16-term and 8 term. We observe that there will be no improvement for accuracy if we still increase terms after 32 terms. Thus, we choose 32 terms to generate the results for α=0.8 and λ=0.1 case.

Table 4.1 - Dimensionless production rate results of α=0.8 and λ=0.1 with different n-terms in GWR inversion.

t_D	n=8	n=16	n=32	n=64	n=128	n=256	n=512
0.001	2.846E+01	2.846E+01	2.846E+01	2.846E+01	2.846E+01	2.846E+01	2.846E+01
0.003	1.428E+01	1.428E+01	1.428E+01	1.428E+01	1.428E+01	1.428E+01	1.428E+01
0.010	7.172E+00	7.172E+00	7.172E+00	7.172E+00	7.172E+00	7.172E+00	7.172E+00
0.032	3.613E+00	3.613E+00	3.613E+00	3.613E+00	3.613E+00	3.613E+00	3.613E+00
0.100	1.792E+00	1.792E+00	1.792E+00	1.792E+00	1.792E+00	1.792E+00	1.792E+00
0.316	6.919E-01	6.919E-01	6.919E-01	6.919E-01	6.919E-01	6.919E-01	6.919E-01
1.000	1.271E-01	1.271E-01	1.271E-01	1.271E-01	1.271E-01	1.271E-01	1.271E-01
3.162	9.642E-03	9.619E-03	9.619E-03	9.619E-03	9.619E-03	9.619E-03	9.619E-03
10.000	4.608E-04	4.614E-04	4.614E-04	4.614E-04	4.614E-04	4.614E-04	4.614E-04
31.623	5.879E-06	5.991E-06	5.991E-06	5.991E-06	5.991E-06	5.991E-06	5.991E-06
100.000	-1.000E-08	7.760E-10	7.759E-10	7.759E-10	7.759E-10	7.759E-10	7.759E-10

Table 4.2 - Difference percentage (%) of difference between current n-terms and half of n-terms (α=0.8 and λ=0.1).

t_D	n=16	n=32	n=64	n=128	n=256	n=512
0.001	1.32E-05	0.00	0.00	0.00	0.00	0.00
0.003	4.62E-06	0.00	0.00	0.00	0.00	0.00
0.010	3.63E-07	0.00	0.00	0.00	0.00	0.00
0.032	5.56E-06	0.00	0.00	0.00	0.00	0.00
0.100	2.32E-04	0.00	0.00	0.00	0.00	0.00
0.316	1.01E-04	0.00	0.00	0.00	0.00	0.00
1.000	2.88E-04	0.00	0.00	0.00	0.00	0.00
3.162	2.39E-01	5.20E-08	0.00	0.00	0.00	0.00
10.000	1.38E-01	2.41E-06	0.00	0.00	0.00	0.00
31.623	1.87E+00	1.96E-05	0.00	0.00	0.00	0.00
100.000	1.39E+03	1.12E-02	0.00	0.00	0.00	0.00

In Table 4.3, we observe that the classical diffusion case also needs 256 terms to get accurate results for dimensionless time up to 100. Moreover, when fractional parameter decreases, less terms of GWR algorithm are needed for accurate results. Furthermore, when tempering factor increases, more terms of GWR algorithm are needed to obtain accurate results. In general, when dimensionless production rate curves have a slower decay in boundary-dominated condition, the dimensionless production rate value will be larger at same dimensionless time. Thus, less terms of GWR algorithm will be needed to maintain accuracy.

Table 4.3 - Number of terms needed to obtain accurate result.

Parameters	n-term
α=1.0 λ=0	256
α=0.4 λ=0.1	16
α=0.6 λ=0.1	32
α=0.8 λ=0.1	64
α=0.8 λ=1.0	128
α=0.8 λ=10.0	512

The computational time (CPU time) of some cases is shown in Table 4.4 below. Different computers may yield different results, so we perform all these calculations on one computer without any other tasks performed. The differences in computational time needed with increasing tempering factor is not obvious. However, when the fractional parameter decreases, less computational time is needed. The reason caused this may still be the slow power-law decay of the curve in long term.

Table 4.4 - Computational time (s) of GWR numerical inversion with various fractional parameter and tempering factor under different number of terms.

n-term of GWR	α=1.0 λ=0	α=0.4 λ=0.1	α=0.6 λ=0.1	α =0.8 λ =0.1	α =0.8 λ =1.0	α =0.8 λ =10
8	0.078	0.062	0.078	0.094	0.094	0.094
16	0.234	0.281	0.265	0.312	0.281	0.281
32	0.702	0.780	0.811	0.874	0.811	0.842
64	2.590	2.605	2.699	2.917	2.902	2.917
128	9.937	9.532	10.374	10.905	10.905	10.827
256	40.404	37.222	40.498	42.916	43.540	42.682
512	180.712	159.09	176.250	183.722	186.796	184.315

4.6 Analyze Field Data

After generating the type curves with different fractional parameter, tempering factor, skin factor and aspect ratio, we need to compare our type curves with some field data in order to furtherly analyzing tempered fractional linear flow behavior. Though our model has certain assumptions and thus causing come limitations, we still find some well production data in Eagle Ford tight oil reservoir that shows the validity of our model.

The first well that we analyzed, Well No.1 is a vertical well with bi-wing fracture in Eagle Ford play near Wilson and Gonzales counties. The production data is published by Wang and Liu (2011), and the production history of this well is about 2800 days. Some reservoir parameters are introduced by Wang and Liu (2011) but they have adjusted parameters during history matching process. Thus, we also obtain reservoir parameters for this area from Gong et al. (2013). Firstly, we check if there is obvious skin factor for Well No.1 by plotting reciprocal of production rate versus square root of time as shown in Fig. 4.16 below. In Fig. 4.16, we can see that the trend of the data points does not form a straight line, and it does not pass the origin. Thus, if assuming linear flow for this well, there is skin effect we need to take in count (Wattenbarger et al., 1998; Escobar et al., 2012).

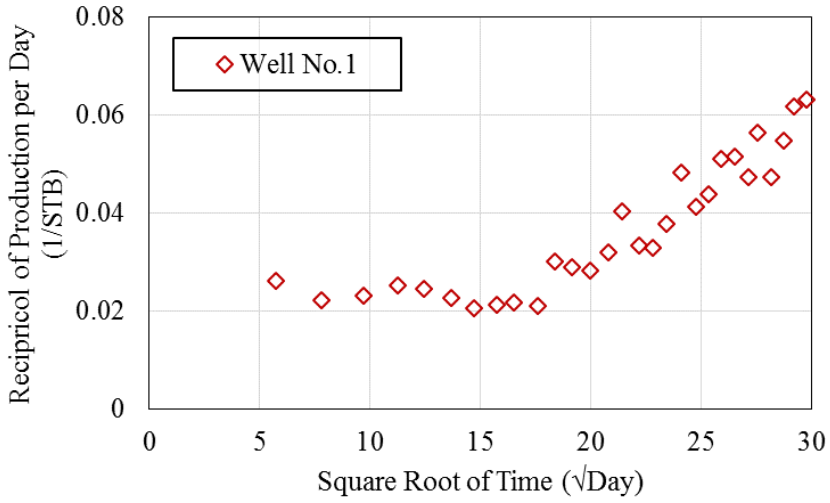

Figure 4.16 - Skin effect check plot for Well No.1 (Short Term).

We calculate dimensionless production rate and dimensionless time for Well No.1 according to the definition introduced in methodology section. The parameters used to calculate the dimensionless variables are adjusted within the reasonable range introduced by Wang and Liu (2011), and Gong et al. (2013). The parameters to calculate dimensionless variables are shown in Table 4.5. We plot the dimensionless results of Well No.1 and results from our tempered fractional linear flow model using α=0.75, λ=6.0, and skin=0.35 in Fig. 4.17. We determine fractional parameter, tempering factor, and skin factor by trail-and-error. In Fig. 4.17, the result from our model matches the dimensionless production data of Well No.1. Some data points deviate from the curve slightly, and this could be caused by well operation or temporary shut-in. Well No.1 shows fast declining rate after reaching boundary dominated condition. Thus, we choose tempering factor 6.0

to match the production data. As discussed in section 4.2 above, tempering factor as large as 6.0 may cause the dimensionless production rate curve having even faster declining rate in long term. Without tempering factor, fractional linear flow model cannot match Well No.1 data for short term and long term at the same time. For Well No.1, we determine the skin factor to be 0.35. For our tempered fractional linear flow model, skin factor of 0.35 is large enough to gloss over the behavior of production rate in short term. Thus, we need to analyze some other wells which does not have long production history but no or small skin effect.

Table 4.5 – Parameters used to calculate dimensionless variables for Well No.1.

Parameter	Value	Unit
Initial reservoir pressure	4200	psi
Well BHP	2000	psi
Reservoir thickness	70	ft
Reservoir permeability	0.009	mD
Reservoir porosity	8%	-
Oil viscosity	0.3	cp
Formation volume factor	1.45	bbl/STB
Total compressibility	1.63×10^{-5}	psi^{-1}
Fracture half-length	160	ft
Aspect ratio	0.727	-

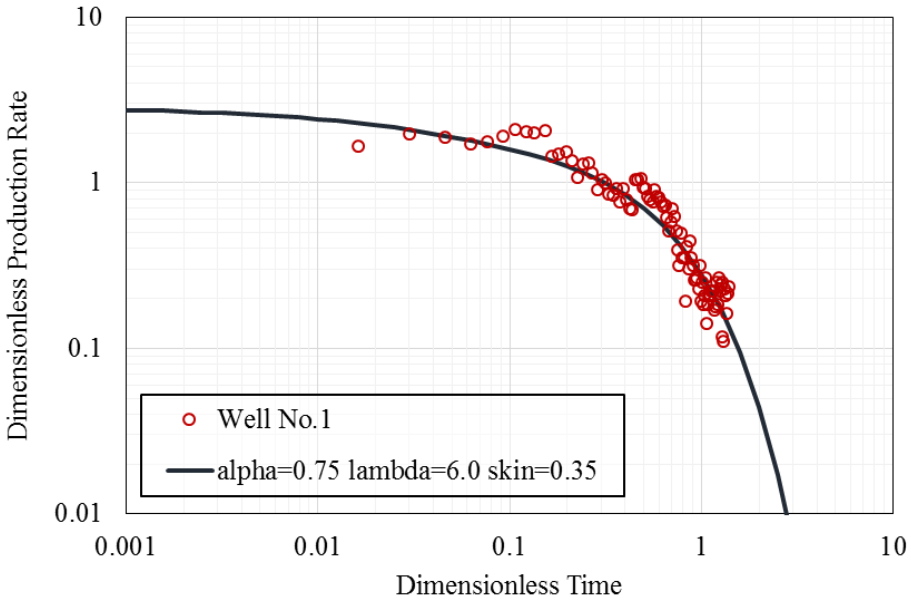

Figure 4.17 - Well No.1 production result compared to our model with $\alpha = 0.75$, $\lambda = 6.0$, *and* $skin = 0.35$.

Agboada and Ahmadi (2013) introduced two multiply fractured horizontal oil wells in Eagle Ford shale play. We name the well from Burleson County as Well No.2, and the well from Dimmit County as Well No.3. These two wells have relatively short production history compared to Well No.1 mention above (Well No.2: 3.5 yrs; Well No.3: 2.5 yrs), and have not received boundary-dominated condition. Thus, we study the application of tempered fractional linear flow model in short term. These two wells have multiple fractures, but they have not reached boundary dominated condition yet. So we can divide the production data by the number of the fractures to obtain the production data from a single fracture. Also, these fractures have identical design so their production rate should be identical.

Firstly, we plot reciprocal of production rate versus square root of time in Fig. 4.18. We can see that the data points in Fig. 4.18 generally follow a straight line, and this straight line has the trend to pass the origin. Thus, we consider no obvious skin effect or very small skin effect that can be neglected.

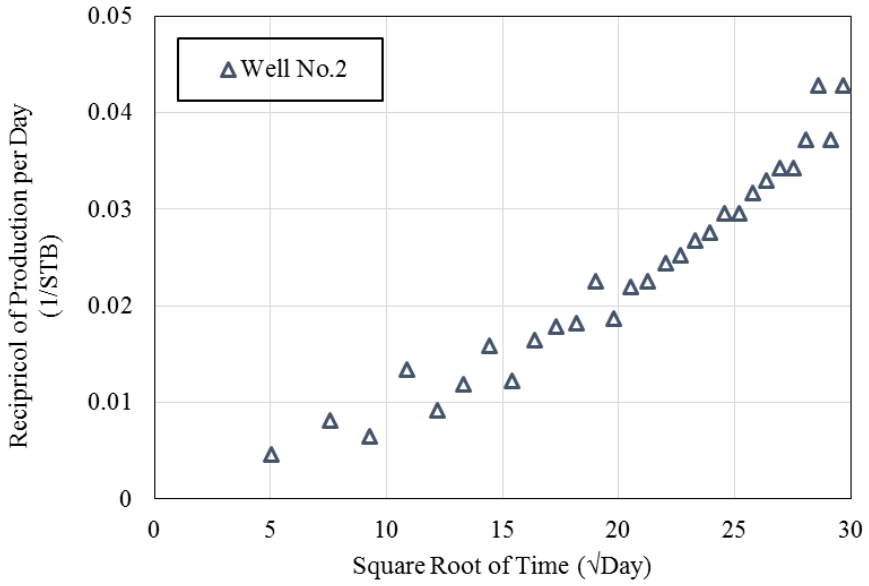

Figure 4.18 - Skin effect check plot for Well No.2.

Agboada and Admadi (2013) showed most of the parameters we need to calculate dimensionless production rate and dimensionless time. The oil viscosity, formation volume factor, and total compressibility are adjusted during the trial-and-error fitting process based on the information from Gong et al. (2013). The parameters used to calculate dimensionless variables in Fig. 4.19, are shown in Table 4.6 below. The aspect

ratio is not important for Well No.2 because the production data is still linear on the log-log plot. Under this condition, the pressure transient has not reach the drainage area boundary, so we cannot estimate the aspect ratio of this drainage area. In order to match with the production data of Well No.2, we use a relatively low fractional parameter and small tempering factor. Also, as discussed above, we set skin factor to be zero as no obvious skin effect is found. In Fig. 4.19, our model matches Well No.2 production data. For Well No.2, tempering factor does not play an important role but it still has effect and let us precisely adjust the linear flow model.

Table 4.6 - Parameters used to calculate dimensionless variables for Well No.2.

Parameter	Value	Unit
Initial reservoir pressure	3800	psi
Well BHP	2850	psi
Reservoir thickness	139	ft
Reservoir permeability	0.00009	mD
Reservoir porosity	4%	-
Oil viscosity	0.3	cp
Formation volume factor	1.3	bbl/STB
Total compressibility	1.33×10^{-5}	psi^{-1}
Fracture half-length	250	ft
Aspect ratio	0.5	-

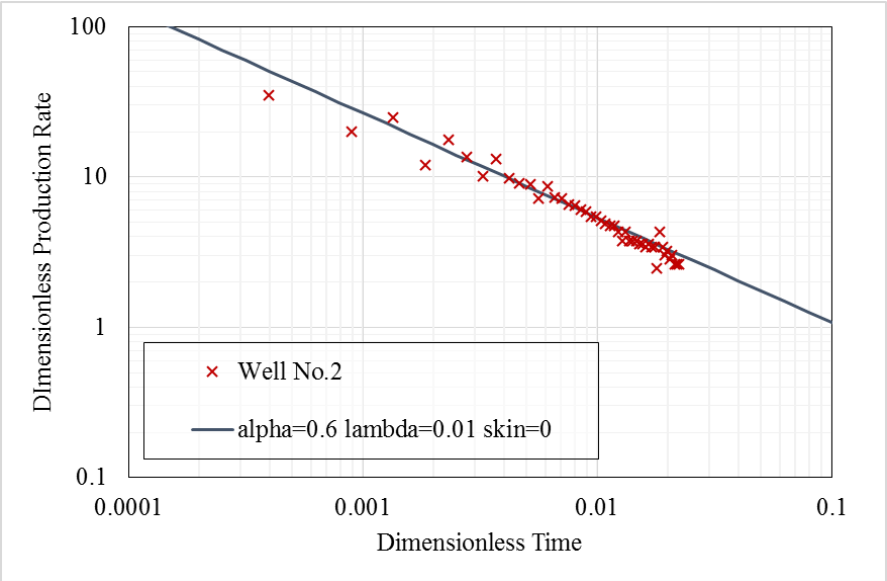

Figure 4.19 - Well No.2 production result compared to our model with $\alpha = 0.6$, $\lambda = 0.01$, *and* $skin = 0$.

In Fig. 4.20, we perform skin effect check for Well No.3. The result shows that the data points fluctuate, and has a linear trend after square root of time of 10. However, the first several data points reveal this well may have small skin factor. Similar as the process of Well No.2, we use most of parameters from Agboada and Admadi (2013). Then, we adjust the rest of parameters based on the reasonable range by Gong et al. (2013). The parameters used to calculate dimensionless variables are shown in Table 4.7 below. Using these parameters, we plot the results of Well No.3 in Fig. 4.21 along with our model's curve ($\alpha = 0.85$, $\lambda = 0.2$, and $\text{skin} = 0.03$). The fist data point of Well No.3 tends to be an outlier so we does not take it into consider while determining skin factor. Apart from few outliers, out model successfully match the production results using the fractional

parameter and tempering factor. Without the help of skin factor, fractional linear flow curve will decline faster in transient period and thus deviate from Well No.3 data.

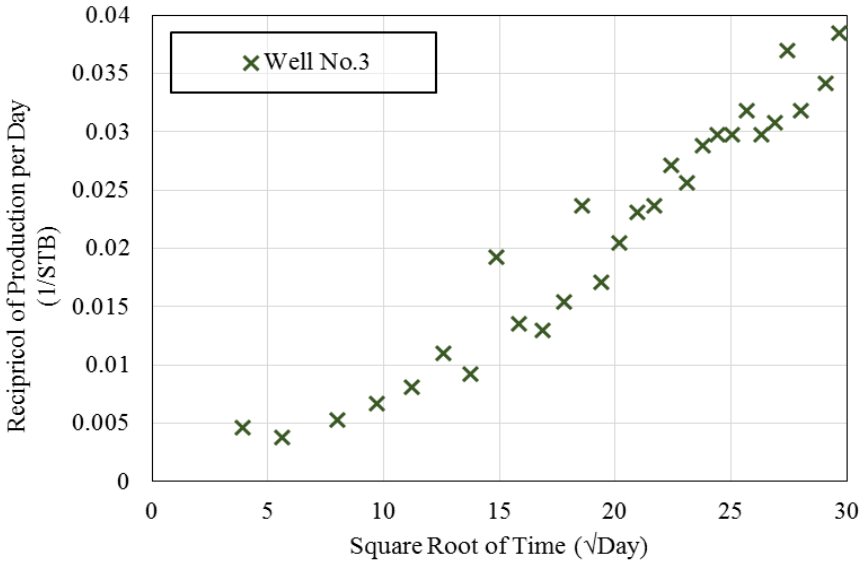

Figure 4.20 - Skin effect check plot for Well No.3.

Table 4.7 - Parameters used to calculate dimensionless variables for Well No.3.

Parameter	Value	Unit
Initial reservoir pressure	3200	psi
Well BHP	1950	psi
Reservoir thickness	147	ft
Reservoir permeability	0.0001	mD
Reservoir porosity	5%	-
Oil viscosity	0.3	cp
Formation volume factor	1.25	bbl/STB
Total compressibility	1.33×10^{-5}	psi^{-1}
Fracture half-length	250	ft
Aspect ratio	0.5	-

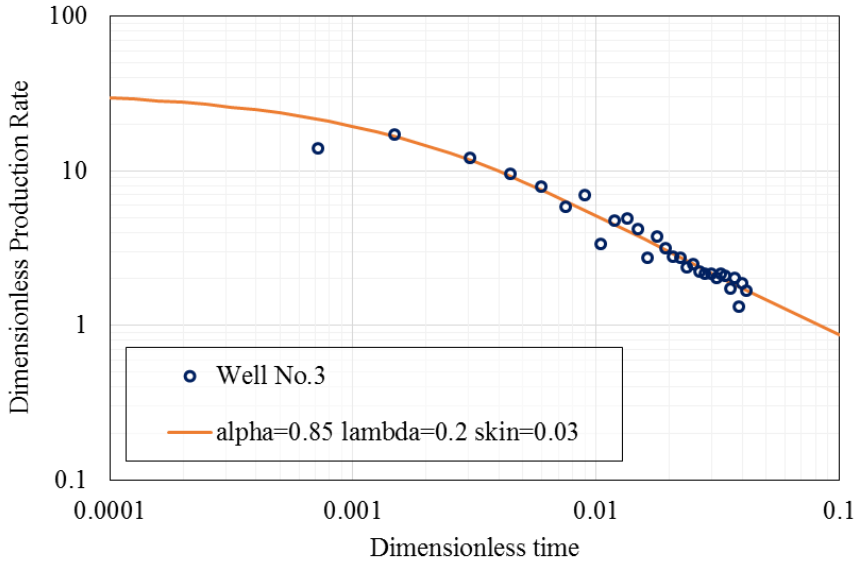

Figure 4.21 - Well No.3 production result compared to our model with $\alpha = 0.85$, $\lambda = 0.2$, *and* $skin = 0.03$.

5. CONCLUSION

In this study, we establish a tempered fractional linear flow model for tight oil reservoir. Our model incorporate skin factor and aspect ratio for versatility. The model uses dimensionless variables in order to generate type curves for tempered fractional linear flow. Two kinds of different inner boundary conditions, including constant rate and constant pressure inner boundary condition, are applied to our model. The tempered fractional linear flow diffusivity equation, and the boundary conditions are transformed into Laplace domain. The solution of dimensionless pressure is firstly obtained in Laplace domain, and then inversely transformed into real time domain numerically using GWR algorithm.

After the model is established, we verify our model with fractional parameter of one and tempering factor of zero with numerical model. Furthermore, our model is verified with Raghavan and Chen's (2017) fractional linear flow model with zero tempering factor under constant rate or constant pressure inner boundary condition. Both comparisons verified the validity of our model. In this case, we continue to generate type curves using our model and furtherly study sub-diffusion behavior.

We study the effect of fractional parameter firstly while keeping tempering factor to be one. We find that smaller fractional parameter results in faster declining of dimensionless production rate in short term, but slower declining of dimensionless production rate in boundary-dominated long term. We also calculate dimensionless productivity index.

When fractional parameter is smaller than one, the dimensionless productivity index curve does not level off after reaching boundary dominated condition.

Secondly, we study the effect of tempering factor, which is novel in our model, and keep fractional parameter to be 0.8. We observe tempering factor successfully temper the power-law behavior of fractional linear flow. In another word, when we increases tempering factor, the dimensionless production rate curve declines faster in boundary-dominated condition. When tempering factor is large enough, the dimensionless production rate curve will decline faster in boundary-dominated condition compared to classical diffusion curve. Before conducting this study, we expect the tempering factor will mainly affect type curves in long term. However, after generating type curves, we observe larger tempering factor results in smaller slope of dimensionless production rate curve in short term. Thus, we conclude that tempering factor is capable to temper fractional linear flow in both short term and long term.

Thirdly, we discuss effect of skin factor and aspect ratio of drainage area. These two factor also have effects on type curves. However, we would like to conclude here is the accuracy and computational time of GWR numerical inversion. We know that more terms of GWR inversion results in higher accuracy. The accuracy we need for different fractional parameters and tempering factors are different. In general, smaller fractional parameter needs less terms to maintain accuracy, while larger tempering factor needs more terms to maintain accuracy. The computational time of GWR inversion is slightly affected by fractional parameter, but keeps constant while we increases tempering factor.

At last, we analyze three fractured oil wells in Eagle Ford shale play. These three wells confirmed the merit of our model. The first well has long enough history, and we find that by adjusting fractional parameter and tempering factor, we can successfully match the sub-diffusion behavior of this well in both short and long term. The other two wells have short production history, and have not reach boundary dominated condition. We observe that tempered fractional linear flow model helps us understanding diffusion behavior which cannot be modeled by classical diffusion.

In a nutshell, we have successfully developed tempered fractional linear flow model, proved its validity, and demonstrated its usefulness to analyze field data. We have some recommendations to future work on this topic. Firstly, our model is designed for oil wells, and this model can be converted to gas wells if using pseudo-pressure instead of real pressure. Secondly, our model is a single fracture model, while it can be furtherly extended to multiply fractured horizontal wells.

NOMENCLATURE

A_f	=	Fracture wing area, ft^2
Ar	=	Rectangular area aspect ratio
B	=	Formation volume factor, bbl/STB
c	=	Compressibility, psi^{-1}
$Const1$	=	Constant 1 used to define skin factor
$Const2$	=	Constant 2 used to define skin factor
$Const3$	=	Constant 3 used to define skin factor
F_{CD}	=	Dimensionless fracture conductivity
h	=	Fracture height, ft
j	=	Gaver functional variable
J_D	=	Dimensionless productivity index
k	=	Rock permeability, md
k_f	=	Fracture permeability, md
L	=	Characteristic distance, ft
L_f	=	Fracture half length, ft
n	=	GWR algorithm variable
p	=	Pressure, psi
p_{ch}	=	Characteristic pressure, psi
p_i	=	Initial reservoir pressure, psi
p_{skin}	=	Pressure drop caused by skin effect, psi

p_{wf}	=	Well flowing bottom-hole pressure, psi
p_D	=	Dimensionless pressure
$\bar{p}_D$	=	Dimensionless pressure in Laplace domain
q	=	Flow rate, bbl/day
q_A	=	Production rate based on drainage area, bbl/day
q_{AD}	=	Dimensionless production rate based on drainage area
q_w	=	Well flow rate, bbl/day
q_{wD}	=	Dimensionless well flow rate
$\bar{q}_D$	=	Dimensionless flow rate in Laplace domain
$\bar{q}_{wD}$	=	Dimensionless production rate in Laplace domain
$\bar{Q}_{wD}$	=	Dimensionless cumulative production in Laplace domain
s	=	Transformed complex variable in Laplace domain
$skin$	=	Skin factor
t	=	Time, day
t_D	=	Dimensionless time
v	=	Flow velocity, ft/s
w_f	=	Fracture width, ft
x	=	Distance from fracture, ft
x_D	=	Dimensionless distance from fracture, ft
x_e	=	Side length (perpendicular to fracture) of rectangular drainage area, ft

x_{eD}	=	Dimensionless side length (perpendicular to fracture) of rectangular drainage area, ft
y_e	=	Side length (parallel to fracture) of rectangular drainage area, ft
y_{eD}	=	Dimensionless side length (parallel to fracture) of rectangular drainage area, ft
α	=	Fractional parameter
λ	=	Tempering factor
ϕ	=	Porosity
τ	=	Gaver functional variable
η	=	Gaver functional variable
ρ	=	GWR algorithm variable

REFERENCES

Agboada, D. K., and Ahmadi, M. (2013, April 19). Production Decline and Numerical Simulation Model Analysis of the Eagle Ford Shale Play. Society of Petroleum Engineers. doi:10.2118/165315-MS

Albinali, A., Holy, R. W., Sarak, H., and Ozkan, E. (2016). Modeling of 1D Anomalous Diffusion in Fractured Nanoporous Media. Oil Gas Science Technology. – Rev. IFP Energies nouvelles. doi: 10.2516/ogst/2016008

Balescu, R., (1998). Strange Diffusion. Condensed Matter Physics 1 (4), 815–833.

Cartea, A., and D. del-Castillo-Negrete (2007), Fluid limit of the continuous time random walk with general Levy jump distribution functions, Phys. Rev. E, 76, 041105.

Chen, C. and Raghavan, R. (2015). Transient flow in a linear reservoir for space–time fractional diffusion. Journal of Petroleum Science and Engineering, Volume 128, Pages 194-202. https://doi.org/10.1016/j.petrol.2015.02.021.

Debnath, L. (2004). "A brief historical introduction to fractional calculus". International Journal of Mathematical Education in Science and Technology. 35 (4): 487–501. doi:10.1080/00207390410001686571.

Escobar, F.H., Roddriguez M.M.R., and Silva, J.H. (2012). Straight-Line Conventional Transient Rate Analysis for Long Homogeneous and Heterogeneous Reservoirs. Directory of Open Access Journals, Volume 79, Number 172, 2012, pp. 156-163(8)

Gong, X., Tian, Y., McVay, D. A., Ayers, W. B., & Lee, J. (2013). Assessment of Eagle Ford Shale Oil and Gas Resources. Society of Petroleum Engineers. doi:10.2118/167241-MS

Holy R. W. (2016). Numerical Investigation of 1D Anomalous Diffusion in Fractured Nanoporous Reservoirs (Doctoral Dissertation). Retrieved from https://dspace.library.colostate.edu/handle/11124/170603

Holy, R. W., & Ozkan, E. (2016a). A Practical and Rigorous Approach for Production Data Analysis in Unconventional Wells. Society of Petroleum Engineers. doi:10.2118/180240-MS

Holy, R. W., & Ozkan, E. (2016b). Numerical Modeling of Multiphase Flow Toward Fractured Horizontal Wells In Heterogeneous Nanoporous Formations. Society of Petroleum Engineers. doi:10.2118/181662-MS

Kelly, J. F., D. Bolster, M. M. Meerschaert, J. D. Drummond, and A. I. Packman (2017), FracFit: A robust parameter estimation tool for fractional calculus models, Water Resour. Res., 53, 2559–2567, doi:10.1002/2016WR019748.

Klages, R., Radons, G., and Sokolov, I. M. (2008). Anomalous Transport: Foundations and Applications. Wiley-VCH Verlag GmbH & Co. KGaA. doi:10.1002/9783527622979

Mathai, A. M. (2006). Special Functions and Functions of Matrix Argument: Recent Advances and Applications in Stochastic Processes, Statistics and Astrophysics. Chapter 3 Fractional Calculus. Centre for Mathematical Sciences, Pala Campus. http://neutrino.aquaphoenix.com/ReactionDiffusion/SERC4chap3.pdf

Meerschaert, M. M., D. A. Benson, H.-P. Scheffler, and B. Baeumer (2002), Stochastic solution of space-time fractional diffusion equations, Phys. Rev. E, 65, 1103–1106.

Meerschaert, M. M., Y. Zhang, and B. Baeumer (2008), Tempered anomalous diffusion in heterogeneous systems, Geophys. Res. Lett., 35, L17403, doi:10.1029/2008GL034899.

Meerschaert, M. M., Sabzikar, F., and Chen, J. (2015). Tempered Fractional Calculus. Journal of Computational Physics, 293, 14–28. http://doi.org/10.1016/j.jcp.2014.04.024

Osada, N. (1990). A Convergence Acceleration Method for Some Logarithmically Convergent Sequences. SIAM Journal on Numerical Analysis, vol. 27, no. 1, pp. 178-189.

Paul, Wolfgang; Baschnagel, Jörg (2013). Stochastic Processes: From Physics to Finance. Springer Science & Business Media. pp. 72–. ISBN 9783319003276. Retrieved 25 July 2014.

Prats, M., Camacho-V, R., & Rodriguez, F. (1997, January 1). One-dimensional Linear Flow With Constant Terminal Pressures. Petroleum Society of Canada. doi:10.2118/97-32

Raghavan, R. (2011). Fractional derivatives: Application to transient flow. Journal of Petroleum Science and Engineering, Volume 80, Issue 1, Pages 7-13. https://doi.org/10.1016/j.petrol.2011.10.003.

Raghavan, R., Chen, C. (2013). Fractional diffusion in rocks produced by horizontal wells with multiple, transverse hydraulic fractures of finite conductivity. Journal of

Petroleum Science and Engineering, Volume 109, Pages 133-143. https://doi.org/10.1016/j.petrol.2013.08.027.

Raghavan, R. (2012). Fractional diffusion: Performance of fractured wells. Journal of Petroleum Science and Engineering, Volumes 92–93, Pages 167-173. https://doi.org/10.1016/j.petrol.2012.06.003.

Raghavan, R. & Chen, C. (2017) Addressing the Influence of a Heterogeneous Matrix on Well Performance in Fractured Rocks. Transport in Porous Media, Volume 117, Pages 69-102. https://doi.org/10.1007/s11242-017-0820-5

Raghavan, R., & Chen, C. (2016, May 5). Rate Decline, Power Laws, and Subdiffusion in Fractured Rocks. Society of Petroleum Engineers. doi:10.2118/180223-MS

Ross, B. (1975). "A brief history and exposition of the fundamental theory of fractional calculus". Fractional Calculus and Its Applications. Lecture Notes in Mathematics. 457: 1–36.

Sabzikar, F., Meerschaert, M. M., and Chen,J (2014). Tempered fractional calculus. Journal of Computational Physics, Volume 293, Pages 14-28. https://doi.org/10.1016/j.jcp.2014.04.

Schmadel, N. M., et al. (2016), Stream solute tracer timescales changing with discharge and reach length confound process interpretation, Water Resour. Res., 52, 3227–3245, doi:10.1002/2015WR018062.

Schumer, R., D. A. Benson, M. M. Meerschaert, and B. Baeumer (2003), Fractal mobile/immobile solute transport, Water Resour. Res., 39(10), 1296, doi:10.1029/2003WR002141.

Valkó, P. P., Abate J. (2002). Comparison of Sequence Accelerators for the Gaver Method of Numerical Laplace Transform Inversion. Computers & Mathematics with Applications, Volume 48, Issues 3–4, Pages 629-636. https://doi.org/10.1016/j.camwa.2002.10.017.

Vlahos, L., Isliker, H., Kominis, Y., and Hizanidis, K. (2008). Normal and Anomalous Diffusion: A Tutorial. Retrieved from https://arxiv.org/abs/0805.0419.

Wattenbarger, R. A., El-Banbi, A. H., Villegas, M. E., & Maggard, J. B. (1998, January 1). Production Analysis of Linear Flow Into Fractured Tight Gas Wells. Society of Petroleum Engineers. doi:10.2118/39931-MS

Wang, J., & Liu, Y. (2011). Well Performance Modeling of Eagle Ford Shale Oil Reservoirs. Society of Petroleum Engineers. doi:10.2118/144427-MS

Zhang, X., and M. Lv (2007), Persistence of anomalous dispersion in uniform porous media demonstrated by pore-scale simulations, Water Resour. Res., 43, W07437, doi:10.1029/2006WR005557.

Zhang, Y., D. A. Benson, and B. Baeumer (2007), Predicting the tails of breakthrough curves in regional-scale alluvial systems, Ground Water, 45(4), 473–484.